International Journal of Nanomedicine

Dovepress
Taylor & Francis Group

Open Access Full Text Article

ORIGINAL RESEARCH

# Biosynthesis and Characterization of ZnO Nanoparticles Using *Citrus reticulata* Peel Followed by Photocatalytic, Antibacterial, and Antioxidative Nanotherapeutic Attributes Assessment Supported by Computer Simulation

Anik Molla[1], Md Minhazul Hoque[1], Fahmida Tasnim Richi[2,3], M Humayan Kabir[1], Safaet Alam[2,4], Nazim Uddin Ahmed[5], Nazim Uddin Emon[6], Chuxiao Shao[7], Chunlai Zeng[8], Shuanghu Wang[7], Peiwu Geng[7], Abdullah Al Mamun[7]

[1]Department of Glass and Ceramic Engineering, Rajshahi University of Engineering and Technology, Rajshahi, 6204, Bangladesh; [2]Department of Pharmaceutical Chemistry, Faculty of Pharmacy, University of Dhaka, Dhaka, 1000, Bangladesh; [3]Department of Pharmacy, University of Asia Pacific, Dhaka, 1215, Bangladesh; [4]Chemical Research Division, BCSIR Dhaka Laboratories, Bangladesh Council of Scientific and Industrial Research (BCSIR), Dhaka, 1205, Bangladesh; [5]Drugs and Toxins Research Division, Bangladesh Council of Scientific and Industrial Research, Rajshahi, Bangladesh; [6]Department of Pharmacy, Faculty of Science and Engineering, International Islamic University Chittagong, Chittagong, 4318, Bangladesh; [7]Central Laboratory of The Lishui Hospital of Wenzhou Medical University, The First Affiliated Hospital of Lishui University, Lishui People's Hospital, Lishui, Zhejiang, 323000, People's Republic of China; [8]Department of Cardiology, Central Laboratory of The Lishui Hospital of Wenzhou Medical University, The First Affiliated Hospital of Lishui University, Lishui People's Hospital, Lishui, Zhejiang, 323000, People's Republic of China

Correspondence: Abdullah Al Mamun, Central Laboratory of The Lishui Hospital of Wenzhou Medical University, The First Affiliated Hospital of Lishui University, Lishui People's Hospital, Lishui, Zhejiang, 323000, People's Republic of China, Tel +86-19715780050, Email pharmaalmamun@yahoo.com



**Introduction:** ZnO nanoparticles (NPs) have garnered significant attention due to their remarkable multifunctionality, particularly in biomedical and environmental applications.

**Methods:** The study synthesized ZnO NPs using *Citrus reticulata* Blanco peel extracts. The structural, morphological, and optical properties of ZnO NPs have been analyzed. The antibacterial and antioxidant activity of ZnO NPs was assessed using disk diffusion and DPPH scavenging method, respectively. Molecular docking was further conducted to support our experiments. In addition, the photocatalytic activity of biosynthesized ZnO NPs was tested using methylene blue (MB) dye.

**Results:** X-ray diffraction (XRD) results indicate that NPs possess a hexagonal wurtzite crystal structure. The crystallite size of the NPs was 30.12 nm. Field emission scanning electron microscopy (FESEM) analysis revealed quasi-spherical and rod-shaped ZnO NPs. Energy Dispersive X-ray (EDX) showed that Zn and O were 86.59% and 13.41% of the total weight, respectively. Optical analysis revealed that the absorption edge was at 373 nm and the band gap was 3.09 eV for ZnO NPs. Moreover, the maximum zone of inhibition was measured at 16.17 ± 0.72 mm, 10.5 ± 0.28 mm, 16.17 ± 0.44 mm, and 12.17 ± 0.44 mm against *Escherichia coli, Staphylococcus aureus, Pseudomonas aeruginosa, and Shigella flexneri*, respectively. Compared with BHT, ZnO NPs showed promising antioxidant performance with an $IC_{50}$ value of 149.01 µg/mL. The photocatalytic efficiency of the ZnO NPs was 6.8%, 8.42%, and 10% after 30, 60, and 90 minutes, respectively. Hesperidin, naringin, rutin, and tangeritin, the principal constituents of *C. reticulata* peel, also showed higher and promising binding affinities against the receptors, with remarkable results compared to the standard in molecular docking analysis. The ADMET analysis also demonstrated that ZnO NPs exhibited low probabilities of hepatotoxicity (3%), nephrotoxicity (20%), and respiratory toxicity (20%), with moderate neurotoxicity (52%).

**Conclusion:** In summary, this study revealed morpho-structural features of green synthesized ZnO NPs and their photodegradation efficiency and bioactivity.

**Keywords:** *Citrus reticulata*, ZnO, nanoparticle, FESEM, XRD, antioxidant, antimicrobial, photocatalytic, molecular docking



Received: 3 October 2024
Accepted: 20 March 2025
Published: 16 April 2025

## Introduction

Since metal oxide nanoparticles, commonly referred to as MONPs, have a wide range of applications in energy, biomedical, electronics, sensor-based technology, solar cells, agriculture, medicine, and catalysis activity-they have ushered in a new era in the field of material science. The unparallel attributes of metal oxide nanoparticles emerge from their quantum confinement effects, scarce gravitational attraction, large active surface area, and strong electromagnetic field, resulting in the enhanced capacity to transfer heat, react as catalysts, exhibit exponential optical properties, and uphold chemical stability.[1–3] In the range of metal oxide nanoparticles, ZnO nanoparticles (NPs) have emerged as a promising candidate due to their wide band gap (BG) of 3.7 eV and high excitation binding energy of 60 meV at ambient temperature.[4] Owing to these properties, ZnO NPs, an n-type semiconductor, have been used in cutting-edge technologies of the modern era, such as gas sensors, solar cells, UV lasers, piezoelectric generators, memory devices, photodetectors, transistors, and spintronics.[5–7] Biocompatibility and non-toxicity are unique features of ZnO NPs that make them suitable for biomedical applications. ZnO NPs have been shown to have a variety of applications, such as in drug delivery, cancer treatment, and wound healing.[8]

Bacterial diseases are often considered a significant concern in developing countries since they cause frequent illness and death among humans. The highly contagious nature of such diseases often makes the situation intractable.[9] Hence, the quest for suitable antibacterial therapeutics is burgeoning day by day in biomedical industries. The organic antibacterial agents that are available now have limitations, such as thermal instability, short lifespan, and faster breakdown rate. In contrast, inorganic microbial-resistant compounds are free from such disadvantages. ZnO NPs are effective inorganic antimicrobial agents that have a tremendous capacity to combat death-causing bacteria.[10] ZnO NPs have been widely recognized for their antioxidant potential. Recent advancements in green synthesis have highlighted the enhanced antioxidant properties of ZnO NPs synthesized using various biological resources, including *Coptidis rhizoma, Berberis aristata*, olive, and *Eucalyptus globulus*. These findings underscore the significance of biogenic approaches in tailoring the functional properties of ZnO NPs for biomedical applications.[11–13]

The scarcity of clean water is an immediate issue worldwide that certainly affects the health and well-being of billions of lives. Waste disposal from various sectors, including agriculture, medicine, textile, and other industries, causes severe water contamination. The significant degradation of water quality renders it unsuitable for drinking or using. The current situation has compelled the world to seek sustainable paths to access water free of contaminants.[14,15] Over the decades, enormous methods such as adsorption, membrane separation, and coagulation have been adopted to remove pollutants from water. However, these approaches have been inadequate regarding persistent organic pollutants.[16] Nonetheless, semiconductor oxide has gained immense familiarity as it efficiently decomposes organic contaminants by photocatalysis.[17] Zinc oxide nanoparticles have remarkable photodegradation efficiency via a heterogenous photocatalysis mechanism, whereby they form reactive oxygen species (ROS) with potent capability of breaking down pollutants. Above all, the diminutive surface area and wide band gap of ZnO NPs render a reduced recombination rate that enhances its potential as a promising photocatalyst.[5,7,18]

Researchers have explored various chemical and physical routes for synthesizing nanoparticles. For example, precipitation, emulsion, solvothermal, hydrothermal, sol-gel, organo-metallic synthesis, spray pyrolysis, thermal evaporation, microwave methods, mechanical milling, molecular beam epitaxy, sputtering, pulsed laser deposition, infrared irradiation, thermal decomposition, plasma irradiation, and ultrasonic irradiation are the most frequently used methods.[19–22] However, there are many initial drawbacks to these methods. The toxic and harmful compounds employed in the chemical approaches have eventually become an enormous threat to our environment. In addition, the incorporation of state-of-the-art equipment and a substantial amount of energy supply is often required, bringing about a rise in the cost of the nanoparticle fabrication process.[20,23,24] Addressing all the limitations, therefore, researchers are turning to new nanoparticle synthesis methods. The green synthesis route, indeed, has gained massive attention in recent times on that ground. The green or biological route is a noble approach for nanoparticle synthesis whose initial aim is to eliminate toxic and perilous chemicals, reduce overall cost, and maintain sustainability. This eco-friendly method involves using various biological substances from plant roots, leaves, flowers, and microorganisms, including algae and bacteria, that contain phytochemicals such as flavonoids, polyphenols, terpenoids, alkaloids which serve both as reducing and capping agents.[25–27] Prior findings demonstrated that nanoparticles

synthesized by green route exhibited outstanding antibacterial properties compared to conventional methods due to the presence of these phytochemicals. In addition, the green route of nanoparticle synthesis emphasizes using benign solvents such as water ($H_2O$) and ethanol ($C_2H_6O$), which is one of the critical objectives of green chemistry.[28]

The exponential growth of the world population has resulted in a massive increase in agricultural waste production across the globe. Hence, the global community addresses waste management as a pressing issue and seeks a sustainable solution to turning waste into a boon. Citrus is a familiar fruit family in the tropical and subtropical countries of Asia. Among 17 species of citrus fruits, *Citrus reticulata*, primarily referred to as mandarin or tangerine, is a prominent one.[29] According to a study in 2016, a large quantity of citrus fruit, over 88 million tons, was produced worldwide.[30] The statistics at the present day have burgeoned exponentially, leading to a waste issue. Utilizing agricultural fruit waste for the biosynthesis of nanoparticles would be a promising solution.[31] Moreover, *C. reticulata* is an abundant source of phytochemical compounds (alkaloids, phenolic acid, flavonoids, limonoids, phenolic esters, triterpenoids, thiamine, volatile oils, and organic acids) that serve as effective reducing and capping agents in green synthesis. Furthermore, these compounds are responsible for significant anticancer, antioxidant, and antibacterial properties of NPs.[9,29,32] Hesperidin (C1), naringin (C2), rutin (C3), and tangeritin (C4) are reported as the main constituents, making up about 86% of the total phenolics extracted from *C. reticulata* peel.[29]

The key objective of our study is to employ a sustainable and eco-friendly route to synthesize ZnO NPs and investigate their promising applications in biomedical and environmental aspects. Hence, the biosynthesis of ZnO NPs has been carried out using *C. reticulata*, commonly known as mandarin orange peel extracts, as a reducing and capping agent. Previously Z. Vasiljevic et al[33] have investigated the synthesis of ZnO NPs using *Citrus sinensis* and *Citrus reticulata* peel extracts, focusing on both biological and photocatalytic activities. However, our study distinguishes itself employing a variant of *C. reticulata*, known as BARI Komla-1, which is quite familiar in Bangladesh.[34] Additionally, our work follows a modified synthesis protocol for ZnO NPs. Furthermore, we have adopted an alternative method for evaluating antioxidant properties and assessed photocatalytic efficiency using methylene blue dye, contrasting with the acid green dye used in earlier study. This study further evaluated the antibacterial activity of ZnO NPs against *Pseudomonas aeruginosa* and *Shigella flexneri*, which are absent in the compared work. In addition, this study incorporates molecular docking and ADMET (Absorption, Distribution, Metabolism, Excretion, and Toxicity) predictions to complement and substantiate the experimental findings on ZnO NPs. Along with ZnO, the key compounds C1, C2, C3, and C4 from *C. reticulata* peel have been subjected to molecular docking analysis for their prospective antioxidant and antibacterial potentials to assess the supportive relevancy for the biological studies of biosynthesized ZnO NPs using *C. reticulata* peel extract.

# Materials and Methods

## Materials

The precursor materials used in the synthesis of ZnO NPs, including zinc acetate dihydrate $(CH_3COO)_2Zn.2H_2O$) [Merck Specialties, India], sodium hydroxide (NaOH) [Merck Specialties, India], and ethanol [Merck Specialties, India] were assured a high level of purity. *C. reticulata* (mandarin orange) was collected from the local market during winter season. It serves as a source of a reducing agent. *C. reticulata* was identified by Md. Arshed Alam, taxonomist, Department of Botany, University of Rajshahi, Bangladesh. The identification was confirmed against the departmental catalog (Coll. No. 75).

## Preparation of Green Extract

Primarily, the peel of freshly collected *C. reticulata* fruit was rinsed gently with distilled water and kept in the dryer. The dried peel was ground into powder. Subsequently, dried powder was mixed into distilled water at a 1:2 ratio and boiled at 70°C for 1 hour in a water bath. The extract of *C. reticulata* peel was collected by filtering with Whatman No.1 Qualitative Filter Papers. Lastly, the peel extract was stored in refrigeration at a suitable temperature.

## Synthesis of ZnO Nanoparticles

A 0.5 molar solution of zinc acetate dihydrate $(CH_3COO)_2Zn.2H_2O$ was prepared in 100 mL distilled water; thereafter, the *C. reticulata* peel extract was poured into the solution at a 1:5 ratio while continuing stirring on a magnetic stirrer at 40°C temperature. Subsequently, a few drops of NaOH solution were added to adjust the pH of the solution to 7–8. The solution was stirred vigorously for 3 hours using a magnetic stirrer to get a homogenous mixture. The appearance of white precipitation suggests the formation of NPs. Afterward, the resulting mixture was centrifuged at 4000 rpm and washed several times to remove impurities. Then, the collected precipitates were dried at 80°C for 8 hours. The dehydrated sample was placed in a furnace to be calcined at 400°C for 4 h. After well grinding, ZnO NPs were stored for further characterization. Figure 1 depicts a generalized green synthesis process, which we have adopted in this study.

## Characterization of ZnO NPs

Different techniques were employed to investigate the crystalline structure, surface morphology and elemental composition of the biosynthesized ZnO NPs. The crystalline structure of ZnO NPs was revealed using X-ray diffraction (XRD) analysis. A SHIMADZU LabX XRD-6100 (Japan) diffractometer with Cu-Kα radiation (40 kV-30 mA) was employed. The scanning speed was set at 2° per minute, and the radiation was scanned at two theta values ranging from 10° to 80°. The surface morphology and elemental composition were identified using a field emission scanning electron microscope (JTM-800, Japan) coupled with an energy-dispersive X-ray spectroscope. In order to measure optical absorption a UV-vis spectrometer (SP-UV 500DB, Germany) was utilized. The similar instrument was employed to record absorbance spectra during the photocatalytic evaluation.

## Antibacterial Assay of ZnO NPs

The antibacterial activity of biosynthesized ZnO NPs was evaluated by employing the disk diffusion method.[35] The resistance of NPs against Gram-positive such as *Staphylococcus aureus* (ATCC25923) and Gram-negative such as *Escherichia coli* (ATCC25922), *Pseudomonas aeruginosa* (ATCC27853), *Shigella flexneri* (clinical isolate) was observed. All the microbes were embedded in Mueller–Hinton agar and subsequently spread homogenously by disinfected cotton swabs. Whatman paper-made sterilized disks were kept in an agar medium; thereafter, 10 µL of 100, 200, and 300 µg/mL specimens were placed on the disks. Ciprofloxacin (5 µg/disk) and methanol were used as positive and negative controls, respectively. Then, the prepared plates were placed for incubation at 37°C ± 1°C for 24 hours. Finally, the zone of inhibition was measured on an mm scale. The evaluation was carried out three times to ensure the reproducibility.

## Antioxidant Assay of ZnO NPs

The antioxidant activity of biosynthesized ZnO NPs was evaluated by DPPH scavenging assessment, as demonstrated in a study by T. Safawo et al.[36] A methanol solution of DPPH (3 mL) was mixed with 1 mL of ZnO NPs at various concentrations (25, 50, 100, 150, 200 ppm). The mixture was then kept in the darkness for half an hour. An absorbance

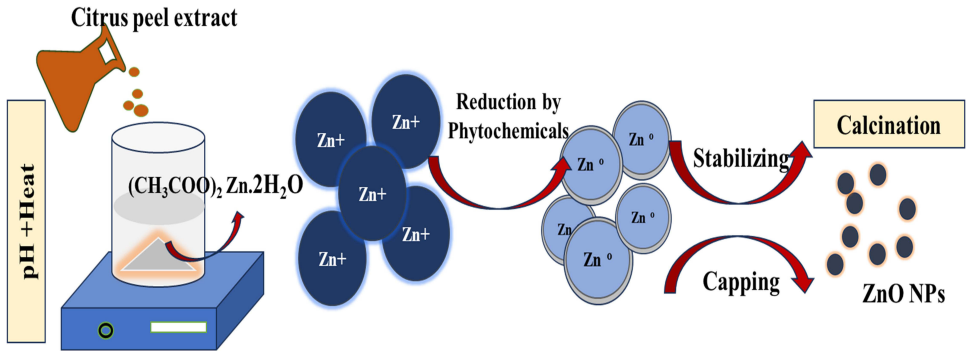


**Figure 1** Represents the mechanism of biosynthesis of ZnO nanoparticles using *Citrus reticulata* peel extract.

spectrum was recorded at 517 nm using a UV spectrophotometer, while Tert-buty-1-hydroxytoluene (BHT) was considered as positive control.

DPPH scavenging activity was measured using the following equation:

$$\text{Scavenging activity}\,(\%) = \left(1 - \frac{\text{Absorbance of sample}}{\text{Absorbance of control}}\right) \times 100\% \quad (1)$$

## Photocatalytic Assay of ZnO NPs

The efficiency of ZnO NPs as a photocatalyst was evaluated by measuring the rate of degradation of methylene blue (MB) dye exposed to UV radiation. A solution of MB dye at a concentration of 15 ppm was prepared by adding the required amount of dye to distilled water. 0.025 gm of the ZnO NPs was mixed with 25 mL of the prepared MB solution in a beaker. Then, the solution was placed in the darkness for 1 hour to become stable. Later, the solution was exposed to UV irradiation in the reactor, while subjected to stirring. At time intervals of 30, 60 and 90 minutes, 5 mL of solution was separated to carry out centrifugation that eventually removed the catalysts. The highest degree of absorbance was calculated from the absorbance spectra plotted using UV-vis spectroscopy within the wavelength range of 400–800 nm. The following equation was used to figure out the rate of degradation:

$$\text{Photodegradation}\,(\%) = \frac{A_0 - A}{A_0} \times 100\% \quad (2)$$

Here, the initial absorbance of the dye solution is denoted as $A_0$, while A represents the absorbance of the dye solution at a specific reaction time.

## In Silico Study: Molecular Docking

### Software

The binding affinities of the selected four compounds from *C. reticulata* against two biologically active target receptor macromolecules were evaluated employing an in-silico approach. A range of software, including Discovery Studio 4.5, Swiss-PDB viewer, PyRx AutoDock Vina (version 1.1.2), and PyMOL 2.3, was employed to assess the molecular interactions comprehensively.

### Target Protein Preparation

The potentials for antioxidant and antibacterial properties of the ligands were investigated. The target macromolecules were obtained as 3D crystal structures from the RCBS Protein Data Bank (https://www.rcsb.org/structure) in the PDB format. For antioxidant and antibacterial activity assessment, glutathione reductase (GLR) [PDB ID: 3GRS][37] and dihydrofolate reductase (DHFR) receptor [PDB ID: 4M6J][38] were employed. Then, with Discovery Studio 2021, all water molecules and heteroatoms were removed from the proteins, followed by Swiss-PDB Viewer's energy minimization tool arranging biomolecules with nonpolar hydrogen atoms, ensuring stable energy states for future research.

### Ligand Preparation

The structures of compounds, namely, hesperidin (C1), naringin (C2), rutin (C3), and tangeritin (C4), along with the standard drug molecules, were downloaded from the PubChem database (https://pubchem.ncbi.nlm.nih.gov/). The ligands were downloaded in the 3D SDF format and serially loaded in the Discovery Studio 4.5. To improve the docking accuracy, a semiempirical technique was used to optimize all the Phyto-constituents.[39] The ZnO NPs were also subjected to molecular docking studies against the target macromolecules. The hexagonal crystal structure of ZnO was acquired from the Materials Project database.

### Ligand–Protein Interaction

Using a computer-aided ligand–protein interaction diagram, the probable binding patterns and binding affinities have been predicted to provide insights into the chemical interactions between molecules. PyRx AutoDock Vina, a very advanced program, was used for the molecular drug-protein linking process. In order to achieve accurate target docking,

a meticulous selection of specific amino acids, and their matching IDs was made from the scientific literature for each receptor separately. Following this, the protein was ready by loading and structuring as the required macromolecule, ensuring targeted ligand binding.

Using PyRx AutoDock Vina software's Open Babel tool, ligand SD files were imported and converted into pdbqt format to improve the docking process with the selected macromolecules. Grid mapping, which followed predefined center and dimension axes, as shown in Table 1, revealed the active amino sites within certain grid boxes (Table 1). During this stage, essential supportive default functions remained unchanged.[40]

ZnO NPs were also docked against the respective macromolecules GLR and DHFR using PyRx AutoDock Vina software, the dimensions of the grid box, while docking with the receptor GLR, were as follows – for the center, x = 60.8973075341, y = 50.4092743942, z = 15.7346707429 and for the size, x = 39.7734540029, y = 28.4484296239, z = 30.9546585142. The dimensions of the grid box, while docking with the receptor DHFR, were as follows – for the center, x = 5.55074167591, y = −0.438411610047, z = −19.1706880895 and for the size, x = 28.8685166482, y = 40.5768232201, z = 30.5540223485. Lastly, the data were analyzed, and the best 2D and 3D models were predicted using BIOVIA Discovery Studio version 4.5.

## In Silico Study: Toxicity Profiling of ZnO

For the evaluation of toxicity profiling of ZnO, ProTox 3.0 (https://tox.charite.de/protox3/) was employed.

## Statistical Analysis

Statistical analysis was conducted using GraphPad Prism 5.2 (GraphPad Software, Inc., La Jolla, CA, USA), with results presented as the mean ± standard error (SEM). To assess statistical significance, one-way ANOVA followed by Dunnett's test was applied, where $*p < 0.05$, $**p < 0.01$, and $***p < 0.001$ were considered significant.

# Results and Discussion

## X-Ray Diffraction (XRD) Analysis

The structural attributes of biosynthesized ZnO NPs were identified by the X-ray diffraction pattern shown in Figure 2. The prominent peaks coordinating the reflection surface (100), (002), (101), (102), (110), (103), (200), (112), (201), (004), and (202) reveal the hexagonal wurtzite structure of ZnO NPs, which show a comparable alignment with JCPDS

**Table 1** Selection of the Target Site and Grid Mapping of Target Receptors

| Receptors | Standards | Target Binding Sites | References | Grid Box | |
|---|---|---|---|---|---|
| GLR (3GRS) | Butylated hydroxy toluene (BHT) | Ile 26, Gly 27, Gly 29, Ser 30, Gly 31, Val 49, Glu 50, Ser 51, Lys 52, Gly 56, Thr 57, Cys 58, Val 61, Gly 62, Cys 63, Lys 66, Lys 67, Gly 128, His 129, Ala 130, Ala 155, Thr 156, Gly 157, Gly 158, Met 159, Ser 177, Phe 181, Tyr 197, Ile 198, Glu 201, Met 202, Arg 291, Asn 294, Leu 298, Asp 331, Leu 337, Leu 338, Thr 339, Pro 340, Ala 342, Val 370, and Phe 372 | [37] | Center | x = 60.2281929041 |
| | | | | | y = 50.7847066882 |
| | | | | | z = 16.1294597491 |
| | | | | Dimension | x = 45.3056141918 |
| | | | | | y = 30.5173950739 |
| | | | | | z = 32.2433179011 |
| DHFR (4M6J) | Ciprofloxacin | Ala 9, Ile 16, Lys 54, Lys 55, Thr 56, Leu 75, Ser 76, Arg 77, Glu 78, Arg 91, Ser 92, Leu 93, Gly 117, Ser 118, Ser 119, and Val 120 | [38] | Center | x = 3.64995808269 |
| | | | | | y = −4.14237379858 |
| | | | | | z = −17.1454766056 |
| | | | | Dimension | x = 26.7652300259 |
| | | | | | y = 32.2142996732 |
| | | | | | z = 28.6296730353 |

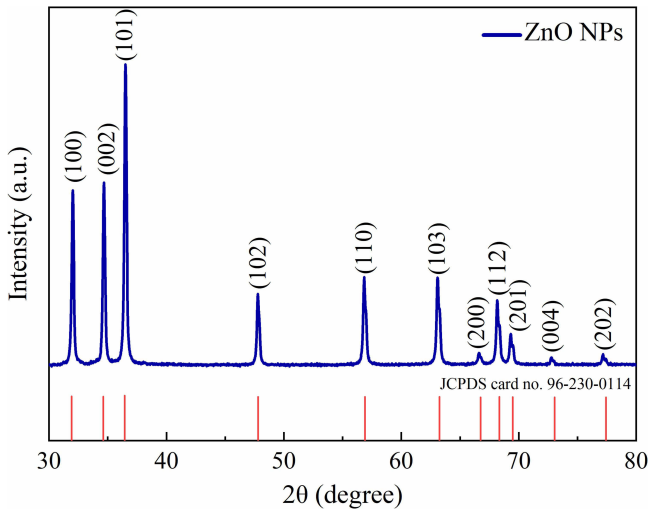


**Figure 2** Represents XRD pattern of biosynthesized ZnO nanoparticles.

card no.96–230-0114 (Table 2). The sharp and narrow peaks of XRD patterns ensure good crystallinity, while the absence of any additional peaks ensures the purity of the NPs.

The polycrystallinity nature of ZnO NPs was identified with the presence of the most acute peak in (101) crystal face.[41–43]

The average crystallite size of ZnO NPs was calculated by Debye–Scherer's Equation (3).[44]

$$D = \frac{k\lambda}{\beta \cos\theta} \tag{3}$$

Here, β = Full width half maxima (FWHM), θ = Bragg angle, λ = wavelength of X-ray (1.5406Å) and k = 0.9.

To calculate the dislocation density, $\delta$ the following equation (4) was adopted, which indicates the concentration of defects in the crystal structure.[45]

**Table 2** Comparison of XRD Data of Biosynthesized ZnO NPs with Standard Value

| Miller Plane (hkl) | JCPDS Card No. 96–230-0114 | | Biosynthesized ZnO NPs | |
|---|---|---|---|---|
| | 2θ | d-spacing (Å) | 2θ | d-spacing (Å) |
| 100 | 31.928 | 2.80073 | 32.02 | 2.793 |
| 002 | 34.625 | 2.58850 | 34.68 | 2.585 |
| 101 | 36.445 | 2.46335 | 36.51 | 2.459 |
| 102 | 47.810 | 1.90095 | 47.81 | 1.901 |
| 110 | 56.898 | 1.61700 | 56.87 | 1.617 |
| 103 | 63.243 | 1.46918 | 63.13 | 1.471 |
| 200 | 66.744 | 1.40036 | 66.65 | 1.402 |
| 112 | 68.345 | 1.37141 | 68.22 | 1.373 |
| 201 | 69.478 | 1.35178 | 69.36 | 1.353 |
| 004 | 73.050 | 1.29425 | 72.82 | 1.298 |
| 202 | 77.424 | 1.23167 | 77.23 | 1.234 |


https://doi.org/10.2147/IJN.S493905

$$\delta = \frac{1}{D^2} \tag{4}$$

The d spacing was measured from Bragg's formula equation (5),

$$2d\sin\theta = n\lambda \tag{5}$$

Here, lattice spacing is indicated by d, θ is the angle of incidence, wavelength is denoted by λ, and n is diffraction order.

The lattice parameters of the hexagonal wurtzite structure of ZnO NPs were calculated by the leading equation.[41]

$$\frac{1}{d^2} = \frac{4}{3} \times \frac{h^2 + hk + k^2}{a^2} + \frac{l^2}{c^2} \tag{6}$$

Where h, k, and l represent the Miller Indices, d is interplanar distance, and a and c are lattice parameters.

Debye–Scherer's method of calculating crystallite size overlooks the value of lattice strain, so it may appear inaccurate. Therefore, crystallite size is calculated using the William Hall method using the formula (7) rendered below. Moreover, the lattice strain was also measured from the plot (Figure 3).

$$\beta \cos\theta = \varepsilon(4 \sin\theta) + \frac{k\lambda}{D} \tag{7}$$

Here, λ denotes the wavelength of dispersion, β assigned to the FWHM (full width at half maximum), θ and ε represent the diffraction angle and strain, respectively.

The slope of the W-H plot confirms that the micro-strain generated in the lattice system is a tensile one, as its value appeared positive.[46] The calculated value for the average crystallite size of NPs is relatively larger (51.73 nm) than that of the Scherrer method (30.12nm).

The plausible reason for that is the consideration of lattice strain in the W-H method. All the calculated structural insights of ZnO NPs are listed in Table 3.

## Morphological and Elemental Analysis

The surface morphology of biosynthesized ZnO NPs was investigated by employing field emission scanning electron microscopy (FESEM). Figure 4 illustrates that ZnO NPs are quasi-spherical and rod-like shaped. The biosynthesized NPs exhibited tendency of agglomeration. The quasi-spherical particles had an average diameter of 48.56 nm, while the rod-shaped particles displayed an average length of 254.36 nm and a width of approximately 114.98 nm. EDX analysis has been carried out to unleash the elemental composition of biosynthesized ZnO NPs. The results suggested that the fundamental elements of NPs were determined to be Zn and O, corresponding to 86.59% and 13.41% of the total weight,

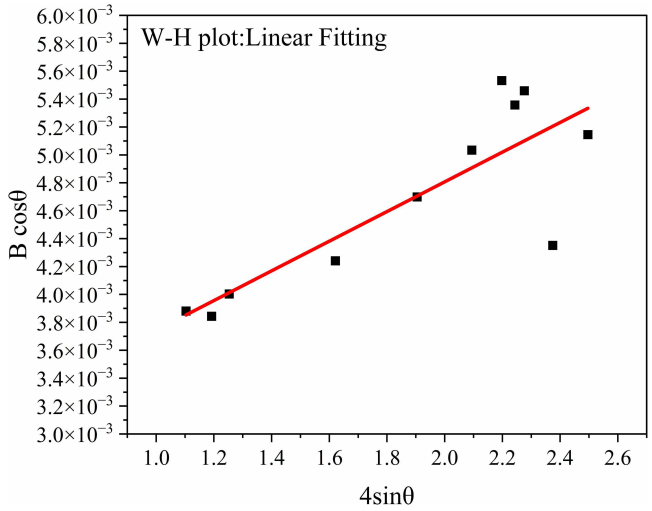


**Figure 3** Represents Williamson-Hall (W-H) plot of ZnO nanoparticles.

**Table 3** The Structural Parameters of ZnO Nanoparticles

| Structural parameters | ZnO NPs |
|---|---|
| Structure | Hexagonal |
| Space group | P63mc |
| FWHM at (101) | 0.24153 |
| d spacing | 2.46 |
| a = b (Å) | 3.23 |
| C (Å) | 5.19 |
| Volume $(Å)^3$ | 46.77 |
| Average crystallite size (Scherrer method) (nm) | 30.12 |
| Crystallite size (W-H method) (nm) | 51.73 |
| Dislocation density, δ $(nm^{-2})$ | 0.001102 |
| Lattice strain, ε | 0.00106 ± 0.000235702 |

respectively (Figure 5). It is noteworthy that the theoretical calculations expected for ZnO NPs are Zn (80.3%) and O (19.7%).[47] Therefore, our results strongly correlate with the fact.

## Optical Property Analysis

Figure 6a represents the UV-visible absorption spectra of biosynthesized ZnO NPs, a widely recognized method to ensure the formation of nanoparticle.[32] In the spectra, the absorption maxima ($\lambda_{max}$) observed at 373 nm correspond to the excitation of electrons from the valence band to the conduction band of ZnO, confirming the formation of ZnO NPs. Moreover, the emergence of a single peak ensured the purity of ZnO NPs. The optical band gap of biosynthesized ZnO NPs, calculated using the Tauc plot (Figure 6b), was found to be 3.09 eV—noticeably lower than that of bulk ZnO.[48] The discernible reduction in the band gap can be attributed to several influencing factors such as crystallite size, particle size and morphology, and calcination temperature.[49,50] To provide a comprehensive context, Table 4 presents the optical properties of ZnO NPs synthesized using different green element and parameters.

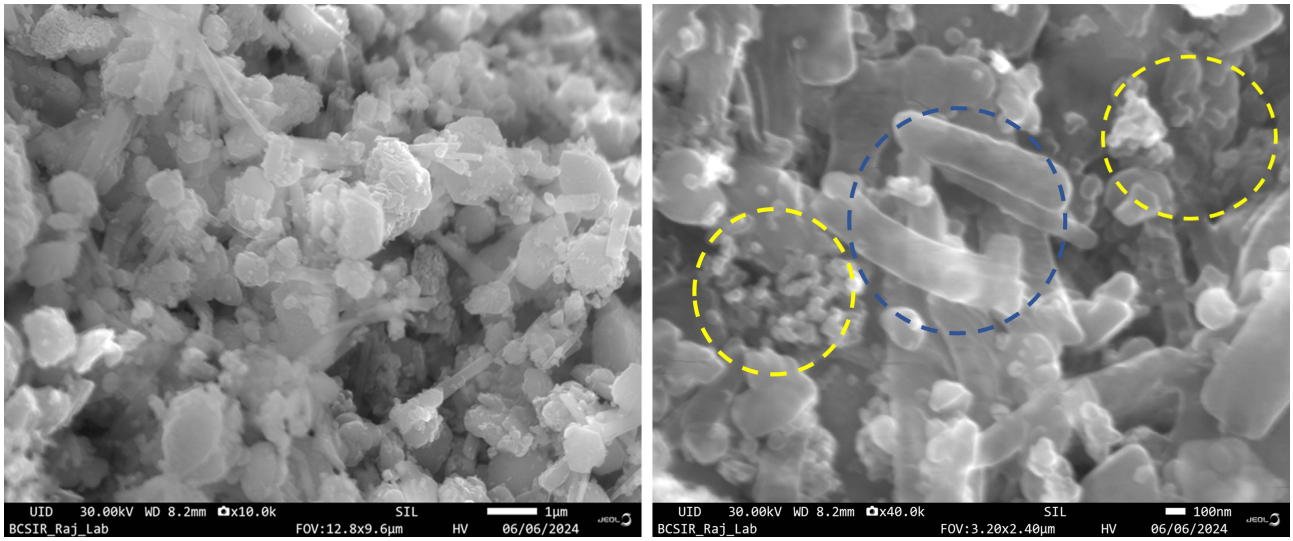


**Figure 4** Represents FESEM image of ZnO NPs where yellow circle indicates the quasi spherical and the blue circles indicates rod like shape.


https://doi.org/10.2147/IJN.S493905

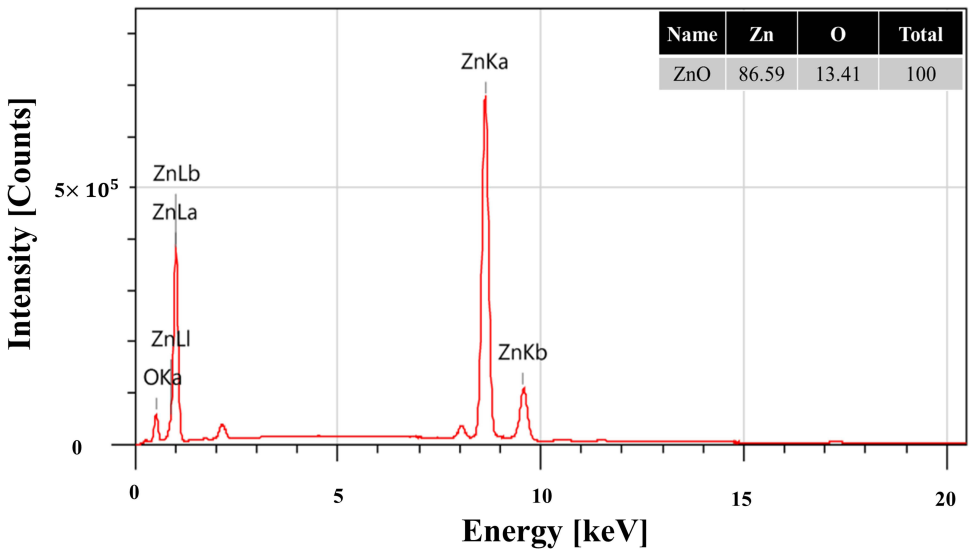


**Figure 5** Represent EDX spectrum of ZnO nanoparticles indicating the presence of compositional elements.

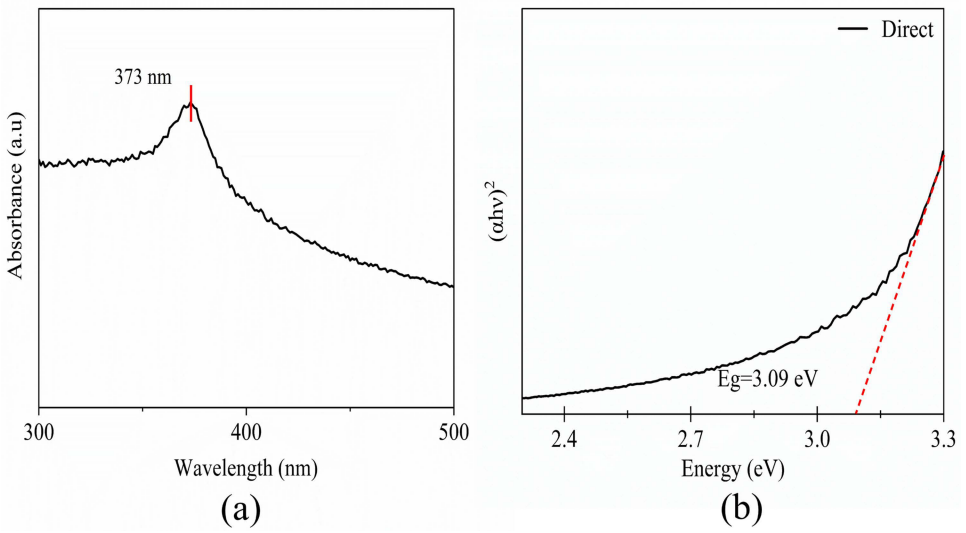


**Figure 6** Represents (**a**) optical absorption and (**b**) the Tauc plot of ZnO nanoparticles.

## Antibacterial Activity

The antibacterial activity of ZnO NPs synthesized using *C. reticulata* peel extract was evaluated against both Gram-positive (*Staphylococcus aureus*) and Gram-negative (*Escherichia coli, Pseudomonas aeruginosa, Shigella flexneri*)

**Table 4** Optical Properties of ZnO Nanoparticles Synthesized from Various Green Element Extracts

| Green Element | Particle Size | Calcination | | Absorption Maxima | Band Gap | Ref. |
|---|---|---|---|---|---|---|
| | | Temperature | Time | | | |
| Brocolli extract | 14 nm | 450 °C | 1 hour | 303 nm | 4.09eV | [42] |
| Tomato extract | >38 nm | 600 °C | 3 hours | 392 nm | 3.16 eV | [51] |
| *Sansevieria trifasciata* root extract | 20 nm | 650 °C | 3 hours | 365 nm | 3.13 eV | [52] |

(*Continued*)

**Table 4** (Continued).

| Green Element | Particle Size | Calcination | | Absorption Maxima | Band Gap | Ref. |
|---|---|---|---|---|---|---|
| | | Temperature | Time | | | |
| Gamboge fruit Extract | 20–30 nm | 410 °C | 2 hours | 370 nm | 3.33 eV | [22] |
| *Myristica fragrans* fruit extract | 43.3 to 83.1 | 500 °C | 2 hours | – | 2.57 eV | [53] |
| *Pisonia Alba* leaf extract | – | 500 °C | 2 hours | 375 nm | 2.96 eV | [54] |

human pathogenic microorganisms. Figure 7 ensures that the NPs showed a remarkable inhibitory zone against those bacteria. It was found that at a dose of 100 µg/mL, the pathogens *E. coli, P. aeruginosa, S. aureus*, and *S. flexneri* had zones of inhibition of 6.17 ± 0.17 mm, 0 ± 0 mm, 7.5 ± 0.28 mm, and 7 ± 0.28 mm, respectively. Further increase of the inhibitory zone was observed at a dose of 200 µg/mL with a zone of inhibition of 11.83 ± 0.44 mm, 8.5 ± 0.28 mm, 12.17 ± 0.44 mm, and 10.5 ± 0.28 mm against *E. coli, S. aureus, P. aeruginosa, and S. flexneri*, respectively (Table 5). At 300 µg/mL, the NPs exhibited notable resistance against *E. coli, S. aureus, P. aeruginosa*, and *S. flexneri*. The measured zones of inhibition were 16.17 ± 0.72 mm, 10.5 ± 0.28 mm, 16.17 ± 0.44 mm, and 12 ± 0.44 mm, correspondingly (Table 5).

It is discernible that the NPs exhibited better resistance against Gram-negative bacteria than that of Gram-positive ones. The structural and compositional differences between Gram-negative and Gram-positive bacteria are considered the prime reason behind that phenomenon. Gram-negative bacteria, for instance, *E. coli and P. aeruginosa* have a thinner

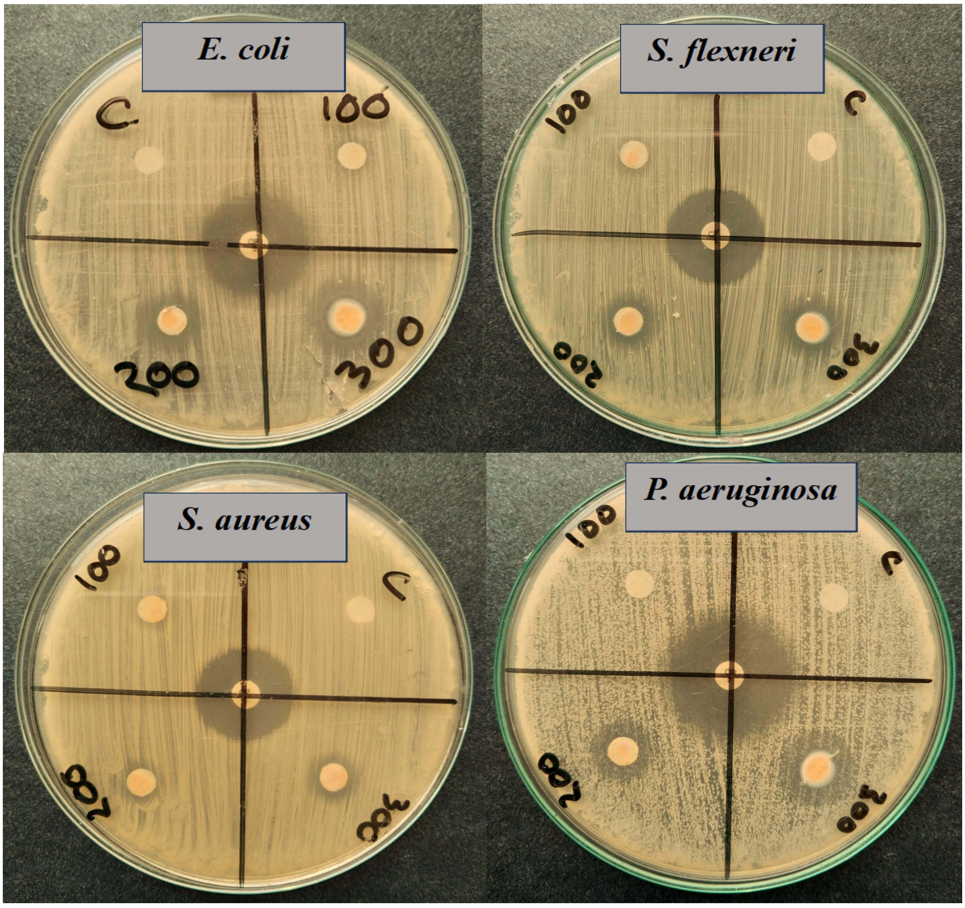


**Figure 7** Represents the zone of inhibition of ZnO NPs against different human pathogenic bacteria.


https://doi.org/10.2147/IJN.S493905

**Table 5** Zone of Inhibition (Mm) of ZnO NPs Against Human Pathogenic Bacteria

| Name of Bacteria | Zone of Inhibition (mm) | | | | |
|---|---|---|---|---|---|
| | Ciprofloxacin 5µg/mL (Positive Control) | Methanol (Negative Control) | 100µg/mL | 200µg/mL | 300µg/mL |
| *Escherichia coli* | 26.67 ± 0.88*** | 0# | 6.17 ± 0.17*** | 11.83 ± 0.44*** | 16.17 ± 0.72*** |
| *Staphylococcus aureus* | 30.83 ± 0.44*** | 0# | 7.5 ± 0.28*** | 8.5 ± 0.28*** | 10.5 ± 0.28** |
| *Pseudomonas aeruginosa* | 26.67 ± 0.88*** | 0# | 0 | 12.17 ± 0.44*** | 16.17 ± 0.44*** |
| *Shigella flexneri* | 25 ± 0.57*** | 0# | 7 ± 0.28*** | 10.5 ± 0.28*** | 12.17 ± 0.44*** |

**Notes**: Data are represented as Mean ± SEM (n = 3). When comparing the data to the control group, Dunnett's *t*-test reveals statistical significance at **$p < 0.01$, and *** $p < 0.001$, along with # denotes control to be compared with.

peptidoglycan cell membrane.[55,56] However, the proposal lacks a strong foundation and requires thorough investigation and supporting evidence. The gradual enhancement of the inhibitory zone and concentration confirms that the antibacterial activity of NPs is a concentration-dependent phenomenon.

Antibacterial resistance of NPs is size and shape-dependent. It is well-defined that NPs, synthesized by various methods, appeared with a notable inhibitory zone against different bacteria when the size of particles is below 100 nm. ZnO NPs with a size range of 12 nm showed unparalleled resistance against *S. aureus* as it not only restricted bacterial growth but also exterminated it utterly.[57] The zone of inhibition of ZnO NPs (average size: 25.97 nm) was shown to be 14.5 mm against *E. coli*.[46] ZnO NPs were synthesized using *Myristica fragrans* extracts; the resulting size ranged from 43.3 to 83.1 nm. An evident notable inhibitory zone was observed against *S. aureus* (14.3 ± 0.7), *P. aeruginosa* (15.6 ± 0.7), *E. coli* (17.3 ± 1.3), *K. pneumoniae* (16.3 ± 0.7).[53] ZnO NPs with a size range of 30–55 nm, synthesized biologically using *Arthrospira platensis* extract, have shown a reasonable degree of resistance against both Gram-positive and Gram-negative microbes such as *Bacillus subtilis* (~24.1), *Staphylococcus aureus* (~21.1), *Pseudomonas aeruginosa* (~19.1), *Escherichia coli* (~19.9), and *Candida albicans* (~21.6) at a concentration of 200 mg/mL.[26]

Previous studies have explained the probable mechanisms of the antibacterial activity of ZnO NPs (Figure 8). The initial microbial cell damage can occur from the frontal attack of ZnO NPs. In the vicinity of water, ZnO NPs generate soluble $Zn^{2+}$ ions that alter the pH level of bacterial cells. Eventually, a specific disruption of cell function happens.

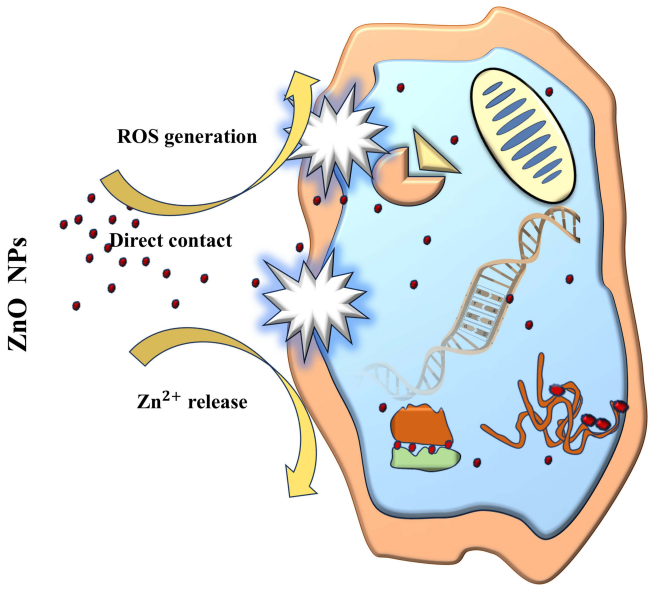


**Figure 8** Represents the mechanism of antibacterial resistance of ZnO nanoparticles.

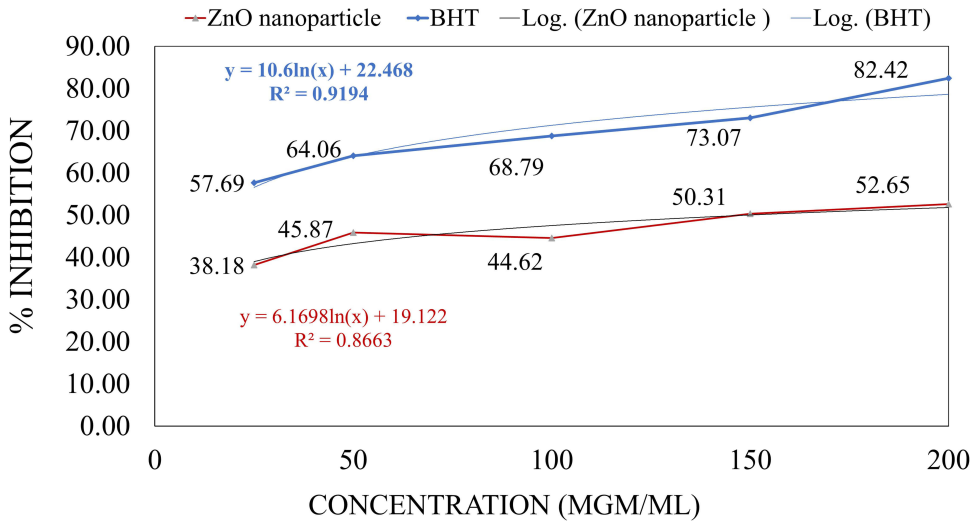


**Figure 9** Represents the rate of inhibition of BHT and ZnO nanoparticles at different concentrations (25, 50, 100, 150, 200 mg/mL).

Notably, the solubility of $Zn^{2+}$ ions is size-dependent and maintains an inverse relationship. Finally, the most prominent mechanism denotes the formation of reactive oxygen species (ROS). Up to a threshold point, the generation of ROS can be stabilized by the antioxidants produced in the bacterial cell. However, a significant rise in ROS generation occurs in large-scale oxidative stress that results in the breaking down of the cellular components into fragments.[57–60]

## Antioxidants Activity

The widely regarded DPPH scavenging technique was employed to assess the antioxidant activity of ZnO NPs. Figure 9 demonstrates the inhibition rate for BHT (standard) and ZnO NPs at various concentrations. The results denote that the percentage of inhibition gradually increases with respect to the concentration elevation. The absorbance of BHT, ZnO nanoparticles and control with respect to concentration is presented in Table 6. The measured $IC_{50}$ value for the positive control, BHT, was determined to be 13.43 µg/mL, whereas the $IC_{50}$ value for ZnO NPs was found to be 149.01 µg/mL (Table 7).

In the metabolic process, a high degree of reactive oxygen species (ROS), such as superoxide, hydroxyl, and peroxy radicals with unpaired electrons, can emerge, leading to disruption in cell functionality and potentially causing severe health issues.[61] In the biological route of nanoparticle synthesis, green elements are used as reducing agents, which are abundant in phytochemicals that are a remarkable source of antioxidants. As mentioned earlier, *C. reticulata* peel is an

**Table 6** Concentration and Corresponding Absorbance of BHT (Butylated Hydroxytoluene), ZnO Nanoparticle and Control

| Concentration (µg/mL) | Absorbance | | |
|---|---|---|---|
| | BHT | ZnO Nanoparticle | Control |
| 200 | 0.312 ± 0.005*** | 0.831 ± 0.004*** | 1.775 ± 0.003# |
| 150 | 0.478 ± 0.003*** | 0.872 ± 0.005*** | 1.775 ± 0.003# |
| 100 | 0.554 ± 0.005*** | 0.972 ± 0.012*** | 1.775 ± 0.003# |
| 50 | 0.638 ± 0.016*** | 0.950 ± 0.002*** | 1.775 ± 0.003# |
| 25 | 0.751 ± 0.014*** | 1.085 ± 0.005*** | 1.775 ± 0.003# |

**Notes**: Data are represented as Mean ± SEM (n = 3). When comparing the data to the control group, Dunnett's *t*-test reveals statistical significance at *** $p < 0.001$, along with # denotes control to be compared with.


https://doi.org/10.2147/IJN.S493905

**Table 7** Value of $IC_{50}$ of BHT (Butylated Hydroxytoluene) and Biosynthesized ZnO Nanoparticles

| Compound | Value of $IC_{50}$ (µg/ mL) |
|---|---|
| BHT | 13.43 |
| ZnO NPs | 149.01 |

excellent reservoir of flavonoids, polyphenols, terpenoids, and alkaloids. Such substance has a tremendous ability to inhibit the radicals that are built in our body. Flavonoids and polyphenols, in particular, are noteworthy in this regard.[62,63] The larger active surface area of ZnO NPs absorbs a high degree of antioxidant substance present in the citrus fruit peel extract, which eventually renders an enhanced rate of inhibition of free radicals by creating a shell of antioxidant substance around the NPs.[64] Scavenging of free radicals by ZnO NPs occurs while the electron of oxygen (outer shell) transfers to the DPPH that neutralizes the radicals.[13] ZnO NPs were synthesized successfully using *Ceropegia candelabrum, Coccinia abyssinica*, and *Solanum nigrum*. The value of $IC_{50}$ of those NPs was observed at 95.09 µg/mL, 127.74 µg/mL, and 126.14 µg/mL, respectively.[36,64,65]

## Photocatalytic Activity

An investigation has been carried out to determine the photodegradation efficiency of ZnO NPs using methylene blue (MB) dye exposed to UV irradiation under different time intervals (0–90 min). It was observed from the absorbance spectra of MB in Figure 10a that the peak height at 664 nm declines along with time intervals, which indicates the photodegradation of MB by ZnO NPs. The disappearance of MB was recorded at 30-minute, 60-minute, and 90-minute periods. Figure 10b shows that the degradation of MB by ZnO was 6.8%, 8.42%, and 10%, respectively.

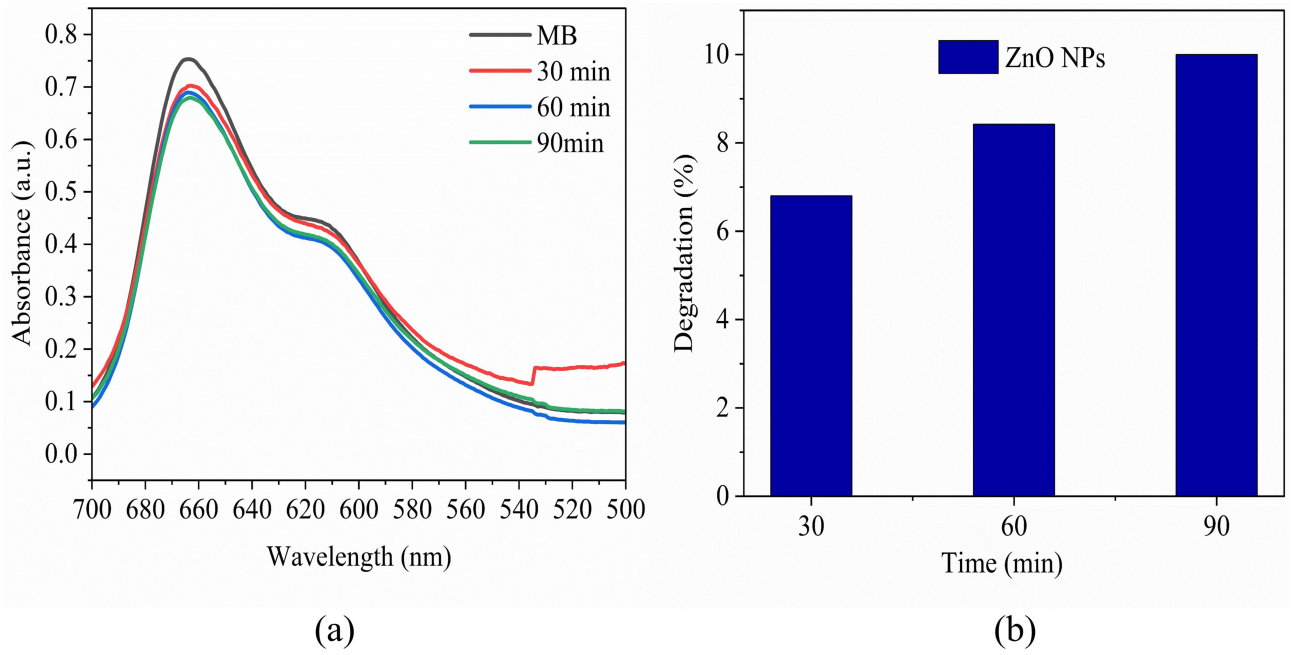


**Figure 10** Represents the photocatalytic activity of biosynthesized ZnO nanoparticles (**a**) absorbance vs wavelength spectra (**b**) plot of degradation (%) vs time (min).

The equations (8–15) stated below render a comprehensive description of the photocatalytic degradation mechanism of methylene blue (MB) dye using ZnO NPs as exposed to UV light,

$$ZnO + UV\,irradiation \rightarrow ZnO\,(e^{-}{}_{CB}) + ZnO\,(h^{+}{}_{VB}) \quad (8)$$

$$ZnO\,(h^{+}{}_{VB}) + H_2O \rightarrow ZnO + H^{+} + OH^{\cdot} \quad (9)$$

$$ZnO\,(h^{+}{}_{VB}) + OH^{-} \rightarrow ZnO + OH^{\cdot} \quad (10)$$

$$ZnO\,(e^{-}{}_{CB}) + O_2 \rightarrow ZnO + O_2{}^{-} \quad (11)$$

$$H^{+} + O_2{}^{-} \rightarrow HO_2{}^{\cdot} \quad (12)$$

$$HO_2{}^{\cdot} + HO_2{}^{\cdot} \rightarrow H_2O_2 + O_2 \quad (13)$$

$$H_2O_2 + O_2{}^{-} \rightarrow OH^{\cdot} + OH^{-} \quad (14)$$

$$Methylene\,Blue\,(MB)\,Dye + OH^{\cdot} \rightarrow Decomposition \quad (15)$$

which is further illustrated in Figure 11.[46,66,67]

As per the illustration, the process of generating electron–hole (e-/$h^{+}$) pairs begins with UV light irradiation. Whenever the energy of irradiated UV light is equal to or beyond the energy of the band gap (BG) of ZnO NPs, a shift of electrons ($e^{-}$) occurs from the valence band (VB) to the conduction band (CB) where they form electron–hole ($e^{-}/h^{+}$) pairs. The reaction is followed up by a redox reaction in the presence of water and oxygen. An oxidation reaction of water with priorly generated holes ($h^{+}$) leads to the formation of OH radicals, while the reduction reaction between oxygen and electrons ($e^{-}$) present in CB converts in OH radical from hydrogen peroxide. Further degradation of dye is encountered from the gradual fading of MB dye color as the interaction between free OH radical and MB dye occurs.

According to our finding, the photocatalytic activity of biosynthesized ZnO NPs was not satisfactory. There might be several underlying reasons as the photocatalytic activity of ZnO NPs is dependent on several factors. One crucial factor is the band gap energy, which significantly influences photocatalytic efficiency. In our case, the absorption maxima (λmax) observed at 373 nm confirmed the formation of ZnO NPs, and the calculated band gap was lower than that of bulk ZnO,

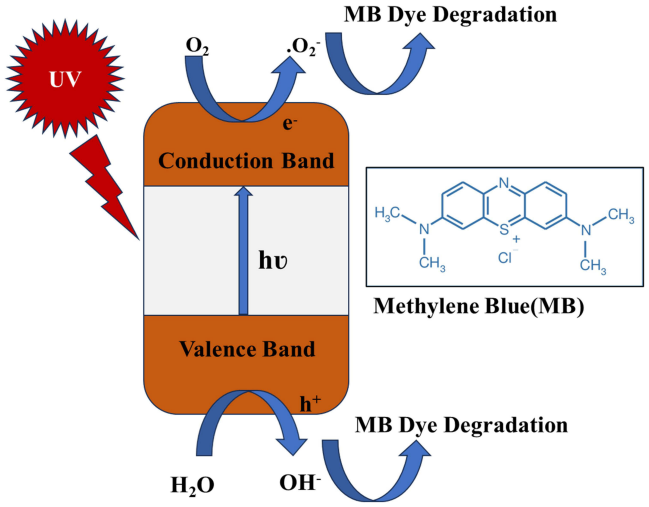


**Figure 11** Represents the mechanism of Methyl Blue (MB) dye degradation by ZnO nanoparticles.


https://doi.org/10.2147/IJN.S493905

theoretically creating favorable conditions for photocatalytic activity.[68] However, the degradation of methylene blue (MB) dye in the presence of these ZnO NPs was notably slow.

Particle size and shape of nanoparticles play a crucial role in the degradation efficiency. The diminutive particle size of nanoparticles provides an enhanced surface area that is available for photocatalytic reaction with MB, thereby leading to an elevation of photocatalytic efficiency.[69] Variations in the shape of NPs influence dye photodegradation in the presence of ZnO NPs. Spherical-shaped NPs exhibited notable efficacy compared to rod-shaped and spindle-shaped NPs due to their enhanced active surface area.[67] In our findings, it is discernible that our synthesized ZnO NPs do not possess superior shape homogeneity. Although, there have been observed diminutive spherical particles, yet the presence of rod shape ZnO NPs were found. Moreover, the particle size was beyond 100 nm in some cases. Besides, the biosynthesized NPs possess the tendency of agglomeration. It can be a probable reason for the lower photocatalytic activity of ZnO NPs. However, the size and shape uniformity nanoparticles are influenced by a complex interplay of factors. Green elements, functioning as reducing and capping agents, are pivotal in this process, with their type and quantity playing a significant role. Moreover, synthesis conditions such as pH and temperature critically affect particle dimensions. Notably, prior studies have revealed that elevated calcination temperature and prolonged duration further contribute to changes in particle size.[70,71] Previously, a slower degradation of 13% of RhB dye was observed under 120 minutes in the presence of ZnO NPs.[72] ZnO NPs, green synthesized using *Garcinia xanthochymus*, have shown a negligible decomposition of MB dye when exposed to UV irradiation. The degree of efficiency was less than 20% after 90 minutes.[48]

## In Silico Study: Molecular Docking

Upon in silico study, the binding affinity of the selected vital compounds from *C. reticulata* peel towards the GLR target is depicted in Table 5. For the receptor GLR, C1, C2, C3, C4, ZnO NPs showed significant binding scores of −11.1, −9.7, −8.9, −7.1 and −3.6 kcal/mol, respectively, while compared to the standard BHT with a binding score of −5.8 kcal/mol.

Among the four compounds, hesperidin (C1) deciphered the highest binding affinity with interactions of pi-cation, pi-anion, pi-sigma, alkyl, conventional hydrogen bond, and carbon-hydrogen bond with amino acids (Table 6 and Figure 12). The 3D and 2D graphical representations of the molecular interactions of these compounds, ZnO and the standard BHT with GLR enzyme are depicted in Figures 12–14.

Glutathione reductase (GLR) is one of the key enzymes in cellular antioxidant defense. It keeps the ratio of oxidized to reduced glutathione in check, which is essential for maintaining redox equilibrium and shielding cells from oxidative stress. An important cellular antioxidant, glutathione disulfide (GSSG), is reduced by this enzyme to its sulfhydryl form (GSH).[73] Researching the interactions between ligands and GLR may help develop treatments for oxidative stress-related illnesses such as cancer, cardiovascular disease, and neurological problems.[74] Antioxidants promote GLR activity, maintain the general health and functionality of cells, and may provide protection against a number of disorders associated with oxidative stress. The combined antioxidant actions of BHT and GLR can provide enhanced protection against oxidative damage, supporting overall cellular health.[75] The promising binding affinities of the aforementioned vital compounds of *C. reticulata* peel and ZnO NPs against the GLR receptor might explain why ZnO NPs decipher antioxidant potential.

Furthermore, in a computational molecular docking study, the standard drug Ciprofloxacin showed −8.2 kcal/mol binding affinity for the DHFR receptor. At the same time, hesperidin (C1) exhibited the highest binding score of −10.1 kcal/mol among all the compounds including van der Waals, carbon-hydrogen bond, unfavorable acceptor–acceptor bond, amide-pi stacked bond, alkyl and pi-alkyl bond interactions with the respective amino acids (Tables 8, 9 and Figure 13). The other compounds also demonstrated prominent scores with −9.4 kcal/mol (C2 & C3) and −8.1 kcal/mol (C4) as per Table 8, whereas ZnO NPs exhibited −3.4 kcal/mol binding score while interacting with the respective amino acids summarized in Tables 8 and 9.

The 3D and 2D graphical representations of the molecular interactions of these compounds and the standard Ciprofloxacin with DHFR enzyme are depicted in Figure 13.

DHFR is another crucial enzyme in all living organisms that converts dihydrofolate to tetrahydrofolate using the cofactor NADPH (reduced nicotinamide-adenine dinucleotide phosphate).[76] This process is essential for synthesizing thymidylate, purines, and amino acids. Inhibiting bacterial DHFR disrupts nucleic acid synthesis, resulting in cell

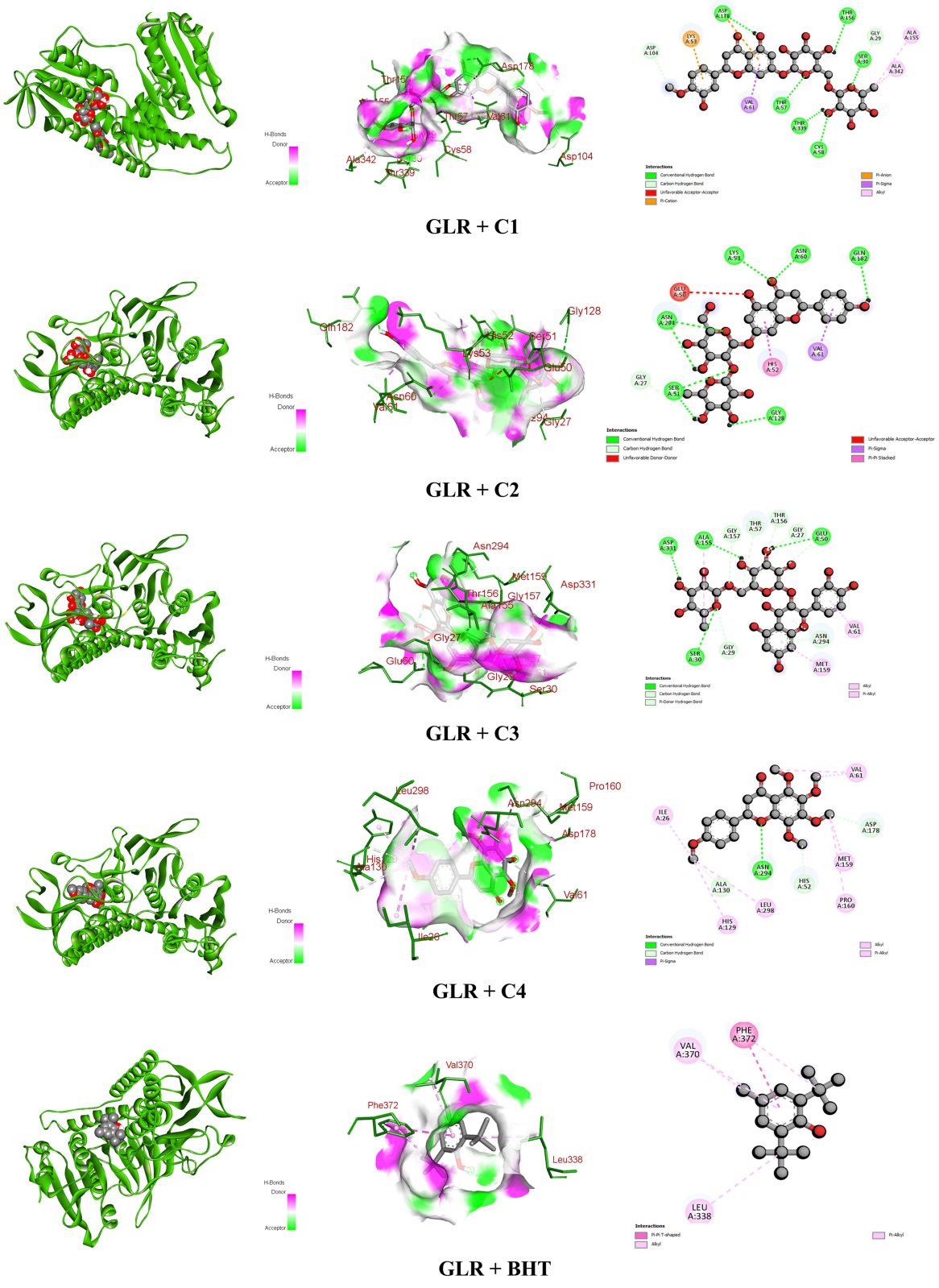


**Figure 12** Graphical representation of the molecular interactions of the selected phytocompounds with the GLR (Glutathione reductase) enzyme with 3D and 2D visualization.


https://doi.org/10.2147/IJN.S493905

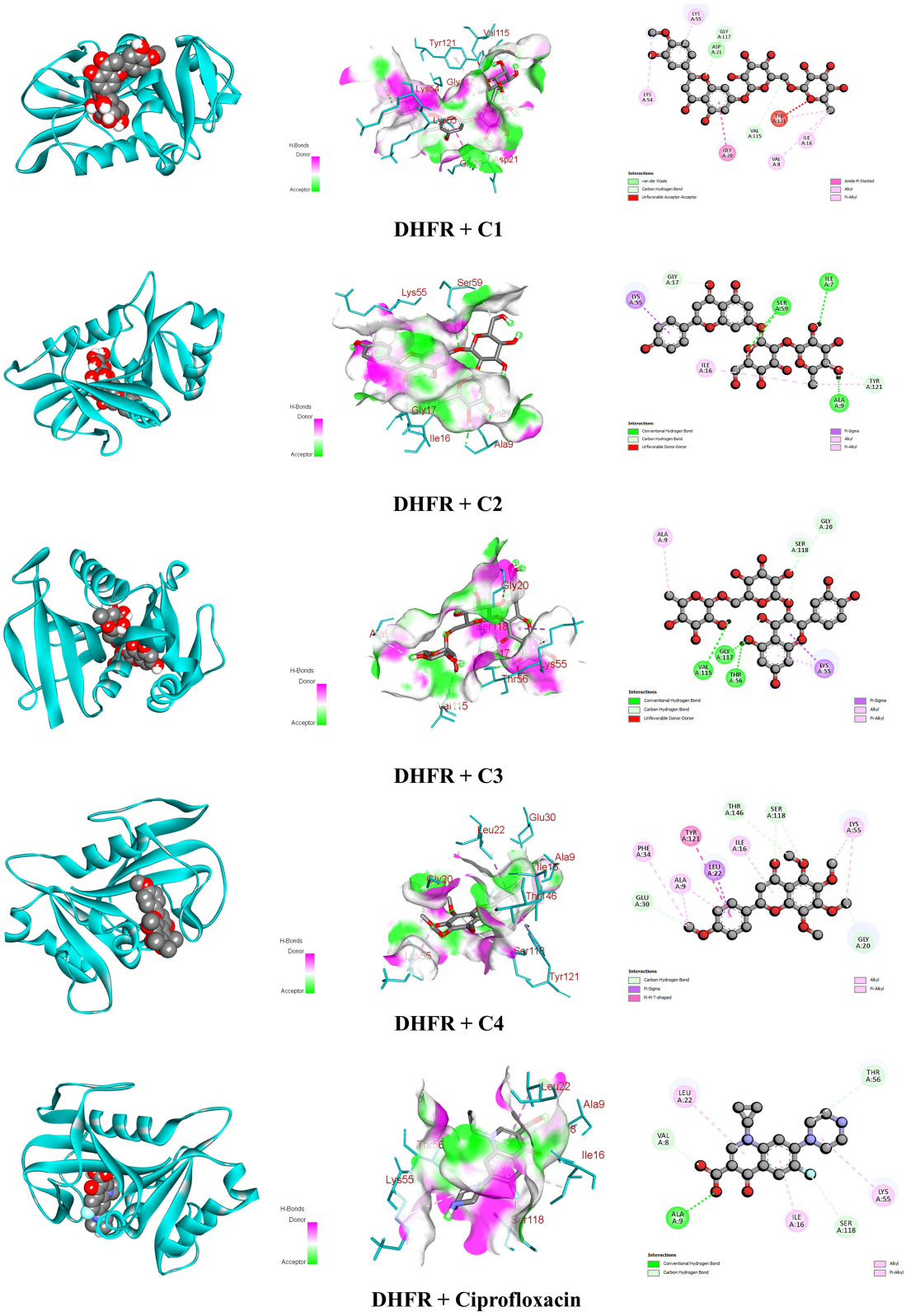


**Figure 13** Graphical representation of the molecular interactions of the selected phytocompounds with the DHFR (dihydrofolate reductase) enzyme with 3D and 2D visualization.

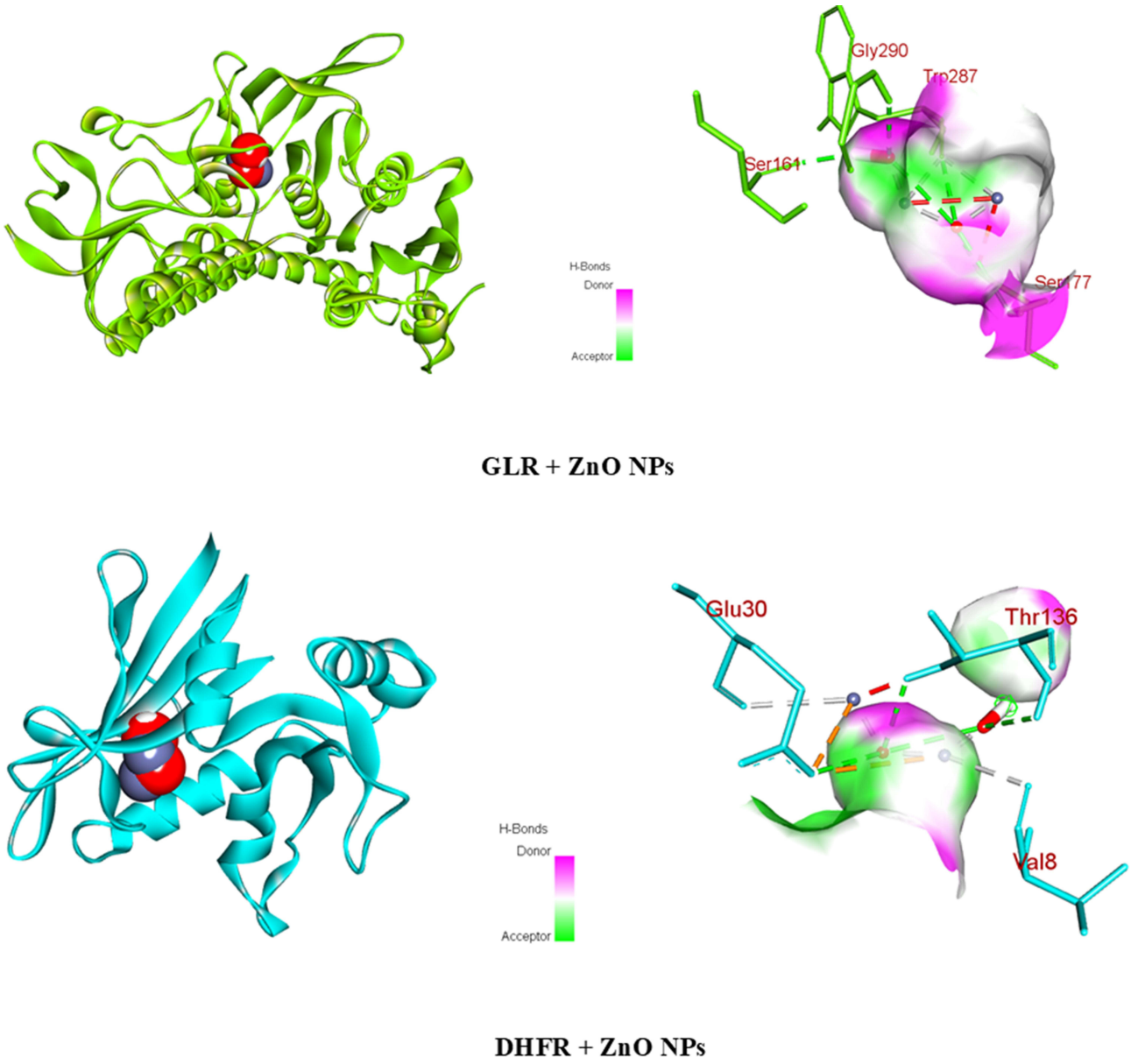


**Figure 14** Graphical representation of the molecular interactions of ZnO nanoparticles with the GLR (Glutathione reductase) and DHFR (dihydrofolate reductase) enzyme with 3D visualization.

death.[77] Ciprofloxacin has the potential to be an antibacterial medication by targeting DHFR, which leads to the death of bacterial cells, effectively treating infections.[78] ZnO NPs might exhibit antibacterial activity because the aforementioned essential components of C. reticulata peel have promising binding affinities against the DHFR receptor.

## In Silico Study: Toxicity Profiling of ZnO

ZnO exhibits low toxicity against most human organ systems as demonstrated in Table 10. It shows inactive hepatotoxicity (97% probability), nephrotoxicity (80%), and respiratory toxicity (80%). However, ZnO presents moderate neurotoxicity (52% probability), indicating some potential for neurological effects. Overall, ZnO demonstrates a relatively safe profile with limited risks to major organs, except for mild neurological concerns. Therefore, the low toxicity profile of ZnO highlights its potential for safe application in nanotherapeutics derived from *C. reticulata* peel. This depicts that the synthesized ZnO NPs can be effectively utilized for photocatalytic, antioxidant, and antibacterial purposes with minimal risk to human health.


https://doi.org/10.2147/IJN.S493905

**Table 8** Binding Affinities of the Selected Compounds from Citrus Reticulata and Respective Standards Against Two Receptors, GLR (Glutathione Reductase) and DHFR (Dihydrofolate Reductase) Representing Antioxidant and Antimicrobial Activities Respectively

| Compound Code | Compound Name | Molecular Weight (g/mol) | Binding Affinity (kcal/mol) | |
|---|---|---|---|---|
| | | | Antioxidant | Antibacterial |
| | | | GLR (3GRS) | DHFR (4M6J) |
| C1 | Hesperidin | 610.6 | −11.1 | −10.1 |
| C2 | Naringin | 580.5 | −9.7 | −9.4 |
| C3 | Rutin | 610.5 | −8.9 | −9.4 |
| C4 | Tangeritin | 372.4 | −7.1 | −8.1 |
| – | ZnO NPs | 81.4 | −3.6 | −3.4 |
| Standards | BHT | 220.35 | −5.8 | – |
| | Ciprofloxacin | 331.34 | – | −8.2 |

**Table 9** Bond and the Binding Site of Identified Best Bounded Compounds from Citrus Reticulata Against Target Receptors, GLR (Glutathione Reductase) and DHFR (Dihydrofolate Reductase)

| Receptor | Compound Code | Binding Affinity (kcal/mol) | Bond Type | Amino Acids |
|---|---|---|---|---|
| | | | | Ser 30, Cys 58, Thr 57, Thr 156, Asp 178, Thr 339 |
| | | | | Gly 29 and Asp 104 |
| | | | Pi-cation | Lys 53 and Asp 178 |
| | | | Pi-anion | Lys 53 and Asp 178 |
| | | | Pi-sigma | Val 61 |
| | | | Alkyl | Ala 155 and Ala 342 |
| | C2 | −9.7 | Conventional hydrogen bond | Ser 51, Lys 53, Asn 60, Gly 128, Gln 182, and Asn 294 |
| | | | Carbon-hydrogen bond | Gly 27 |
| | | | Unfavorable donor-donor | Glu 50 |
| | | | Unfavorable acceptor-acceptor | Glu 50 |
| | | | Pi-sigma | Val 61 |
| | | | Pi-pi stacked | His 52 |
| | C3 | −8.9 | Conventional hydrogen bond | Ser 30, Glu 50, Ala 155, and Asp 331 |
| | | | Carbon-hydrogen bond | Gly 27, Gly 29, Glu 50, Thr 57, and Gly 157 |
| | | | Pi-donor hydrogen bond | Thr 156 and Asn 294 |
| | | | Alkyl | Ala 155 |
| | | | Pi-alkyl | Val 61 and Met 159 |

(*Continued*)

**Table 9** (Continued).

| Receptor | Compound Code | Binding Affinity (kcal/mol) | Bond Type | Amino Acids |
|---|---|---|---|---|
| | C4 | −7.1 | Conventional hydrogen bond | Asn 294 |
| | | | Carbon-hydrogen bond | His 52, Ala 130, and Asp 178 |
| | | | Alkyl | Ile 26, Val 61, His 129, Met 159, Pro 160, and Leu 298 |
| | ZnO NPs | −3.6 | - | Ser 161, Ser 177, Trp 287, and Gly 290 |
| | BHT | −5.8 | Pi-pi T-shaped | Phe 372 |
| | | | Alkyl | Leu 338, Val 370, and Phe 372 |
| | | | Pi-alkyl | Val 370 |
| DHFR (4M6J) | C1 | −10.1 | Van der waals | Asp 21 |
| | | | Carbon-hydrogen bond | Val 115 and Gly 117 |
| | | | Unfavorable acceptor-acceptor | Tyr 121 |
| | | | Amide-pi stacked | Gly 20 |
| | | | Alkyl | Val 8, Ile 16, Lys 54, and Tyr 121 |
| | | | Pi-alkyl | Lys 55 |
| | C2 | −9.4 | Conventional hydrogen bond | Ile 7, Ala 9, and Ser 59 |
| | | | Carbon-hydrogen bond | Ser 59 and Tyr 121 |
| | | | Pi-sigma | Lys 55 |
| | | | Alkyl | Ile 16 and Tyr 121 |
| | C3 | −9.4 | Conventional hydrogen bond | Thr 56, Val 115, and Gly 117 |
| | | | Carbon-hydrogen bond | Gly 20 and Ser 118 |
| | | | Pi-sigma | Lys 55 |
| | | | Alkyl | Ala 9 |
| | | | Pi-alkyl | Lys 55 |
| | C4 | −8.1 | Carbon-hydrogen bond | Glu 30, Ser 118, and Thr 146 |
| | | | Pi-sigma | Leu 22 |
| | | | Pi-pi T-shaped | Tyr 121 |
| | | | Alkyl | Ala 9, Phe 34, and Lys 55 |
| | | | Pi-alkyl | Ala 9 and Ile 16 |
| | ZnO NPs | −3.4 | - | Val 8, Glu 30, and Thr 136 |
| | Ciprofloxacin | −8.2 | Conventional hydrogen bond | Ala 9 |
| | | | Carbon-hydrogen bond | Val 8, Thr 56, and Ser 118 |
| | | | Pi-alkyl | Ile 16, Leu 22, and Lys 55 |


https://doi.org/10.2147/IJN.S493905

**Table 10** Toxicity Profile of ZnO Nanoparticles Against Human Cells

| **Prediction of Toxicity of ZnO** | | | |
|---|---|---|---|
| **Classification** | **Target** | **Prediction** | **Probability** |
| Organ toxicity | Hepatotoxicity | Inactive | 0.97 |
| Organ toxicity | Neurotoxicity | Active | 0.52 |
| Organ toxicity | Nephrotoxicity | Inactive | 0.8 |
| Organ toxicity | Respiratory toxicity | Inactive | 0.80 |
| Organ toxicity | Cardiotoxicity | Inactive | 0.98 |
| Toxicity end points | Carcinogenicity | Inactive | 0.66 |
| Toxicity end points | Immunotoxicity | Inactive | 0.99 |
| Toxicity end points | Mutagenicity | Inactive | 0.59 |
| Toxicity end points | Cytotoxicity | Inactive | 0.79 |
| Toxicity end points | BBB-barrier | Active | 0.99 |
| Toxicity end points | Ecotoxicity | Active | 0.77 |
| Toxicity end points | Clinical toxicity | Inactive | 0.85 |
| Toxicity end points | Nutritional toxicity | Inactive | 0.59 |
| Tox21-Nuclear receptor signaling pathways | Aryl hydrocarbon Receptor (AhR) | Inactive | 0.97 |
| Tox21-Nuclear receptor signaling pathways | Androgen Receptor (AR) | Inactive | 1 |
| Tox21-Nuclear receptor signaling pathways | Androgen Receptor Ligand Binding Domain (AR-LBD) | Inactive | 0.88 |
| Tox21-Nuclear receptor signaling pathways | Aromatase | Inactive | 0.93 |
| Tox21-Nuclear receptor signaling pathways | Estrogen Receptor Alpha (ER) | Inactive | 0.94 |
| Tox21-Nuclear receptor signaling pathways | Estrogen Receptor Ligand Binding Domain (ER-LBD) | Inactive | 0.86 |
| Tox21-Nuclear receptor signaling pathways | Peroxisome Proliferator-Activated Receptor Gamma (PPAR-Gamma) | Inactive | 0.86 |
| Tox21-Stress response pathways | Nuclear factor (erythroid-derived 2)-like 2/antioxidant responsive element (nrf2/ARE) | Inactive | 0.79 |
| Tox21-Stress response pathways | Heat shock factor response element (HSE) | Inactive | 0.79 |
| Tox21-Stress response pathways | Mitochondrial Membrane Potential (MMP) | Inactive | 0.95 |
| Tox21-Stress response pathways | Phosphoprotein (Tumor Suppressor) p53 | Inactive | 0.89 |
| Tox21-Stress response pathways | ATPase family AAA domain-containing protein 5 (ATAD5) | Inactive | 0.88 |
| Molecular Initiating Events | Thyroid hormone receptor alpha (THR$\alpha$) | Inactive | 0.90 |
| Molecular Initiating Events | Thyroid hormone receptor beta (THR$\beta$) | Inactive | 0.78 |

(*Continued*)

**Table 10** (Continued).

| Prediction of Toxicity of ZnO | | | |
|---|---|---|---|
| **Classification** | **Target** | **Prediction** | **Probability** |
| Molecular Initiating Events | Transtyretrin (TTR) | Inactive | 0.97 |
| Molecular Initiating Events | Ryanodine receptor (RYR) | Inactive | 0.98 |
| Molecular Initiating Events | GABA receptor (GABAR) | Inactive | 0.96 |
| Molecular Initiating Events | Glutamate N-methyl-D-aspartate receptor (NMDAR) | Inactive | 0.92 |
| Molecular Initiating Events | Alpha-amino-3-hydroxy-5-methyl-4-isoxazolepropionate receptor (AMPAR) | Inactive | 0.97 |
| Molecular Initiating Events | Kainate receptor (KAR) | Inactive | 0.99 |
| Molecular Initiating Events | Achetylcholinesterase (AChE) | Inactive | 0.97 |
| Molecular Initiating Events | Constitutive androstane receptor (CAR) | Inactive | 0.98 |
| Molecular Initiating Events | Pregnane X receptor (PXR) | Inactive | 0.92 |
| Molecular Initiating Events | NADH-quinone oxidoreductase (NADHOX) | Inactive | 0.97 |
| Molecular Initiating Events | Voltage gated sodium channel (VGSC) | Inactive | 0.95 |
| Molecular Initiating Events | Na+/I- symporter (NIS) | Inactive | 0.98 |
| Metabolism | Cytochrome CYP1A2 | Inactive | 0.96 |
| Metabolism | Cytochrome CYP2C19 | Inactive | 0.95 |
| Metabolism | Cytochrome CYP2C9 | Active | 0.68 |
| Metabolism | Cytochrome CYP2D6 | Inactive | 0.88 |
| Metabolism | Cytochrome CYP3A4 | Inactive | 0.93 |
| Metabolism | Cytochrome CYP2E1 | Inactive | 0.94 |

## Limitations and Future Direction

While our current study offers valuable insights into biosynthesized ZnO NPs, certain limitations must be addressed. This study does not include the emerging challenges in the scalability of ZnO NPs using the green route. The structural and compositional attributes of ZnO NPs were revealed by several techniques, which confirmed the successful synthesis of ZnO NPs. However, by employing several advanced techniques such as TEM, and XPS we might potentially gain a better perspective.[79] The photocatalytic activity was performed in a controlled laboratory setup that does not fully imitate the real-world environment. The photocatalytic efficacy of ZnO NPs was evaluated for only methylene blue dye, while the assessment could be extended for different categories of dyes at various concentration levels. In our work, several preclinical studies, such as the antibacterial and antioxidant activity of ZnO NPs, were carried out. The results are still promising. Further, in vitro bioavailability testing must be conducted to adjudicate future clinical trial studies. In addition, it is necessary to evaluate the safety, efficacy, and toxicity profiles, as these parameters will play a vital role in the assessment of the optimum dose limit of ZnO NPs.[80,81] Our research can be expanded in the future to mitigate the highlighted limitations. On that ground, our current study will act as a linkage, providing useful insights that unleash the potential of biosynthesized ZnO NPs in wastewater management, bacterial resistance, and oxidative stress management. The important findings from several characterizations will contribute to the study's future progress.

## Conclusion

To conclude, the ZnO NPs were biosynthesized using a sustainable and eco-friendly approach. The presence of various phytochemicals in *Citrus reticulata* peel acted as reducing agents as well as stabilizing agents. Various characterization techniques were adopted to analyze the structural, morphological and optical attributes of ZnO NPs. XRD pattern of ZnO confirms the hexagonal wurtzite structure with an average crystallite size of 30.12 nm. The biosynthesized ZnO NPs exhibited relatively larger particle size with irregular shape homogeneity. Both quasi-spherical and rod-like particles were identified by FESEM micrographs. The elemental mapping was carried out by EDX, which showed the successful synthesis of nanoparticles. The optical band gap of ZnO NPs was calculated to be 3.09 eV. The biosynthesized ZnO NPs exhibited promising antibacterial activity against both Gram-positive and Gram-negative bacteria. The maximum zone of inhibition was measured at 16.17 ± 0.72 mm, and 16.17 ± 0.44 mm against *E. coli, and, P. aeruginosa* at concentrations of 300 µg/mL. ZnO NPs were found effective in the inhibition of radicals with an $IC_{50}$ value of 149.01 µg/mL. However, the ZnO NPs exhibited a lower photocatalytic activity. The degradation of MB dye was found to be slower, yet it maintained an upward trend with time intervals. Molecular docking studies that key compound, including hesperidin (C1), exhibited high binding affinities towards GLR (−11.1 kcal/mol) and DHFR (−10.1 kcal/mol), surpassing standard drugs BHT (−5.8 kcal/mol) and Ciprofloxacin (−8.2 kcal/mol), justifying the relevant antioxidant and antibacterial potentials. ZnO nanoparticles displayed low toxicity with probabilities of hepatotoxicity (3%), nephrotoxicity (20%), and respiratory toxicity (20%), but moderate neurotoxicity (52%). These findings highlight the potential of ZnO nanoparticles for safe and effective nanotherapeutic applications targeting oxidative stress and bacterial infections.

## Funding

This study was partially supported by the Key Research & Development Plan of Zhejiang Province (2024C03171), the Zhejiang Provincial Traditional Chinese Medicine Science and Technology Project (2024ZL1302) and the Post-doctoral Research Start-Up Fund of Lishui People's Hospital (2023bsh001), Zhejiang, China.

## Disclosure

The authors report no conflicts of interest in this work.

## References

1. Kalpana VN, Devi Rajeswari V. A review on green synthesis, biomedical applications, and toxicity studies of ZnO NPs. *Bioinorg Chem Appl*. 2018;2018:1–12. doi:10.1155/2018/3569758
2. Ansari A, Siddiqui VU, Rehman WU, et al. Correction: green synthesis of TiO2 nanoparticles using Acorus calamus leaf extract and evaluating its photocatalytic and in vitro antimicrobial activity (Catalysts, (2022), 12, 181), 10.3390/catal12020181). *Catalysts*. 2022;12(11). doi:10.3390/catal1211145
3. Nabi G, Ain QU, Tahir MB, et al. Green synthesis of TiO2 nanoparticles using lemon peel extract: their optical and photocatalytic properties. *Int J Environ Anal Chem*. 2022;102(2):434–442. doi:10.1080/03067319.2020.1722816
4. Nava OJ, Soto-Robles CA, Gómez-Gutiérrez CM, et al. Fruit peel extract mediated green synthesis of zinc oxide nanoparticles. *J mol Struct*. 2017;1147:1–6. doi:10.1016/j.molstruc.2017.06.078
5. Weldegebrieal GK. Synthesis method, antibacterial and photocatalytic activity of ZnO nanoparticles for azo dyes in wastewater treatment: a review. *Inorg Chem Commun*. 2020;120:108140. doi:10.1016/j.inoche.2020.108140
6. Matinise N, Fuku XG, Kaviyarasu K, Mayedwa N, Maaza M. ZnO nanoparticles via Moringa oleifera green synthesis: physical properties & mechanism of formation. *Appl Surf Sci*. 2017;406:339–347. doi:10.1016/j.apsusc.2017.01.219
7. Mclaren A, Valdes-Solis T, Li G, Tsang SC. Shape and size effect of ZnO nanocrystals on photocatalytic activity supporting information. *J Am Chem Soc*. 2009;001:12540–12541. doi:10.1021/ja9052703
8. Davar F, Majedi A, Mirzaei A. Green synthesis of ZnO nanoparticles and its application in the degradation of some dyes. *J Am Ceram Soc*. 2015;98(6):1739–1746. doi:10.1111/jace.13467
9. Saeb S, Amin M, Seyfi Gooybari R, Aghel N. Evaluation of antibacterial activities of citrus limon, citrus reticulata, and citrus grandis against pathogenic bacteria. *Int J Enteric Pathog*. 2016;4(4):11–15. doi:10.15171/ijep.2016.13
10. Fang M, Chen JH, Xu XL, Yang PH, Hildebrand HF. Antibacterial activities of inorganic agents on six bacteria associated with oral infections by two susceptibility tests. *Int J Antimicrob Agents*. 2006;27(6):513–517. doi:10.1016/j.ijantimicag.2006.01.008
11. Nagajyothi PC, Sreekanth TVM, Tettey CO, Jun YI, Mook SH. Characterization, antibacterial, antioxidant, and cytotoxic activities of ZnO nanoparticles using Coptidis Rhizoma. *Bioorganic Med Chem Lett*. 2014;24(17):4298–4303. doi:10.1016/j.bmcl.2014.07.023
12. Chandra H, Patel D, Kumari P, Jangwan JS, Yadav S. Phyto-mediated synthesis of zinc oxide nanoparticles of Berberis aristata: characterization, antioxidant activity and antibacterial activity with special reference to urinary tract pathogens. *Mater Sci Eng C*. 2019;102:212–220. doi:10.1016/j.msec.2019.04.035

13. Siripireddy B, Mandal BK. Facile green synthesis of zinc oxide nanoparticles by Eucalyptus globulus and their photocatalytic and antioxidant activity. *Adv Powder Technol*. 2017;28(3):785–797. doi:10.1016/j.apt.2016.11.026
14. Shannon MA, Bohn PW, Elimelech M, Georgiadis JG, Marĩas BJ, Mayes AM. Science and technology for water purification in the coming decades. *Nature*. 2008;452(7185):301–310. doi:10.1038/nature06599
15. Babuji P, Thirumalaisamy S, Duraisamy K, Periyasamy G. Human health risks due to exposure to water pollution: a review. *Water*. 2023;15(14):1–15. doi:10.3390/w15142532
16. Ong CB, Ng LY, Mohammad AW. A review of ZnO nanoparticles as solar photocatalysts: synthesis, mechanisms and applications. *Renew Sustain Energy Rev*. 2018;81(March 2017):536–551. doi:10.1016/j.rser.2017.08.020
17. Suwarnkar MB, Dhabbe RS, Kadam AN, Garadkar KM. Enhanced photocatalytic activity of Ag doped TiO2 nanoparticles synthesized by a microwave assisted method. *Ceram Int*. 2014;40(4):5489–5496. doi:10.1016/j.ceramint.2013.10.137
18. Zheng X, Shen ZP, Shi L, Cheng R, Yuan DH. Photocatalytic membrane reactors (PMRs) in water treatment: configurations and influencing factors. *Catalysts*. 2017;7(8):224. doi:10.3390/catal7080224
19. Álvarez-chimal R, García-Pérez VI, Álvarez-Pérez MA, Arenas-Alatorre JÁ. Green synthesis of ZnO nanoparticles using a Dysphania ambrosioides extract. Structural characterization and antibacterial properties. *Mater Sci Eng C*. 2021;118:111540. doi:10.1016/j.msec.2020.111540
20. Bandeira M, Giovanela M, Roesch-Ely M, Devine DM, da Silva Crespo J. Green synthesis of zinc oxide nanoparticles: a review of the synthesis methodology and mechanism of formation. *Sustain Chem Pharm*. 2020;15:100223. doi:10.1016/j.scp.2020.100223
21. Diallo A, Ngom BD, Park E, Maaza M. Green synthesis of ZnO nanoparticles by Aspalathus linearis: structural & optical properties. *J Alloys Compd*. 2015;646:425–430. doi:10.1016/j.jallcom.2015.05.242
22. Vijayakumar S, Mahadevan S, Arulmozhi P, Sriram S, Praseetha PK. Green synthesis of zinc oxide nanoparticles using Atalantia monophylla leaf extracts: characterization and antimicrobial analysis. *Mater Sci Semicond Process*. 2018;82(March):39–45. doi:10.1016/j.mssp.2018.03.017
23. Ahmed S, Annu, Chaudhry SA, Ikram S, Ikram S. A review on biogenic synthesis of ZnO nanoparticles using plant extracts and microbes: a prospect towards green chemistry. *J Photochem Photobiol B: Biol*. 2017;166:272–284. doi:10.1016/j.jphotobiol.2016.12.011
24. Upadhyaya H, Shome S, Sarma R, Tewari S, Bhattacharya MK, Panda SK. Green synthesis, characterization and antibacterial activity of ZnO nanoparticles. *Am J Plant Sci*. 2018;9(6):1279–1291. doi:10.4236/ajps.2018.96094
25. Xu J, Huang Y, Zhu S, Abbes N, Jing X, Zhang L. A review of the green synthesis of ZnO nanoparticles using plant extracts and their prospects for application in antibacterial textiles. *J Eng Fiber Fabr*. 2021;16. doi:10.1177/15589250211046242.
26. El-Belely EF, Farag MMS, Said HA, et al. Green synthesis of zinc oxide nanoparticles (Zno-nps) using Arthrospira *platensis* (class: *Cyanophyceae*) and evaluation of their biomedical activities. *Nanomaterials*. 2021;11(1):1–18. doi:10.3390/nano11010095
27. Hussein BY, Mohammed AM. Green synthesis of ZnO nanoparticles in grape extract: their application as anti-cancer and anti-bacterial. *Mater Today Proc*. 2021;42:A18–A26. doi:10.1016/j.matpr.2021.03.729
28. Chan YY, Pang YL, Lim S, Chong WC. Facile green synthesis of ZnO nanoparticles using natural-based materials: properties, mechanism, surface modification and application. *J Environ Chem Eng*. 2021;9(4):105417. doi:10.1016/j.jece.2021.105417
29. Ferreira SS, Silva AM, Nunes FM. Citrus reticulata Blanco peels as a source of antioxidant and anti-proliferative phenolic compounds. *Ind Crops Prod*. 2018;111:141–148. doi:10.1016/j.indcrop.2017.10.009
30. Negro V, Mancini G, Ruggeri B, Fino D. *Citrus Waste as Feedstock for Bio-Based Products Recovery: Review on Limonene Case Study and Energy Valorization*. Vol. 214. 2016. doi:10.1016/j.biortech.2016.05.006
31. Aswathi VP, Meera S, Maria CGA, Nidhin M. Green synthesis of nanoparticles from biodegradable waste extracts and their applications: a critical review. *Nanotechnol Environ Eng*. 2023;8(2):377–397. doi:10.1007/s41204-022-00276-8
32. Sujitha MV, Kannan S. Green synthesis of gold nanoparticles using Citrus fruits (Citrus limon, Citrus reticulata and Citrus sinensis) aqueous extract and its characterization. *Spectrochim Acta - Part a mol Biomol Spectrosc*. 2013;102:15–23. doi:10.1016/j.saa.2012.09.042
33. Vasiljevic Z, Vunduk J, Bartolic D, et al. An eco-friendly approach to ZnO NP synthesis using Citrus reticulata Blanco Peel/extract: characterization and antibacterial and photocatalytic activity. *ACS Appl Bio Mater*. 2024;7(5):3014–3032. doi:10.1021/acsabm.4c00079
34. Alam MD, Abme H, Rahim MA. Fruit yielding plants and their relative preference in the nurseries of greater Dhaka district in Bangladesh. *J Agrofor Env*. 2008;2:1–6.
35. Mie R, Samsudin MW, Din LB, Ahmad A, Ibrahim N, Adnan SNA. Synthesis of silver nanoparticles with antibacterial activity using the lichen Parmotrema praesorediosum. *Int J Nanomed*. 2014;9:121–127. doi:10.2147/IJN.S52306
36. Safawo T, Sandeep BV, Pola S, Tadesse A. Synthesis and characterization of zinc oxide nanoparticles using tuber extract of anchote (Coccinia abyssinica (Lam.) Cong.) for antimicrobial and antioxidant activity assessment. *OpenNano*. 2018;3(August):56–63. doi:10.1016/j.onano.2018.08.001
37. Qiu X, Janson CA, Smith WW, Head M, Lonsdale J, Konstantinidis AK. Refined structures of -ketoacyl-acyl carrier protein synthase III. *J mol Biol*. 2001;307(1):341–356. doi:10.1006/jmbi.2000.4457
38. Khatun MCS, Muhit MA, Hossain MJ, Al-Mansur MA, Rahman SMA. Isolation of phytochemical constituents from Stevia rebaudiana (Bert.) and evaluation of their anticancer, antimicrobial and antioxidant properties via in vitro and in silico approaches. *Heliyon*. 2021;7(12):e08475. doi:10.1016/j.heliyon.2021.e08475
39. Bikadi Z, Hazai E. Application of the PM6 semi-empirical method to modeling proteins enhances docking accuracy of AutoDock. *J Cheminform*. 2009;1(1):15. doi:10.1186/1758-2946-1-15
40. Muhammad N, Lal Shrestha R, Adhikari A, et al. First evidence of the analgesic activity of govaniadine, an alkaloid isolated from *Corydalis govaniana* Wall. *Nat Prod Res*. 2015;29(5):430–437. doi:10.1080/14786419.2014.951933
41. Bhatia S, Verma N. Photocatalytic activity of ZnO nanoparticles with optimization of defects. *Mater Res Bull*. 2017;95:468–476. doi:10.1016/j.materresbull.2017.08.019
42. Osuntokun J, Onwudiwe DC, Ebenso EE. Green synthesis of ZnO nanoparticles using aqueous Brassica oleracea L. var. italica and the photocatalytic activity. *Green Chem Lett Rev*. 2019;12(4):444–457. doi:10.1080/17518253.2019.1687761
43. Sadiq H, Sher F, Sehar S, et al. Green synthesis of ZnO nanoparticles from Syzygium Cumini leaves extract with robust photocatalysis applications. *J mol Liq*. 2021:335. doi:10.1016/j.molliq.2021.116567.
44. Pillai AM, Sivasankarapillai VS, Rahdar A, et al. Green synthesis and characterization of zinc oxide nanoparticles with antibacterial and antifungal activity. *J Mol Struct*. 2020;1211:128107. doi:10.1016/j.molstruc.2020.128107

45. Wasly HS, El-Sadek MSA, Henini M. Influence of reaction time and synthesis temperature on the physical properties of ZnO nanoparticles synthesized by the hydrothermal method. *Appl Phys A*. 2018;124:1–12. doi:10.1007/s00339-017-1482-4
46. Haque MJ, Bellah MM, Hassan MR, Rahman S. Synthesis of ZnO nanoparticles by two different methods & comparison of their structural, antibacterial, photocatalytic and optical properties. *Nano Express*. 2020;1(1). doi:10.1088/2632-959X/ab7a43
47. Fakhari S, Jamzad M, Kabiri Fard H. Green synthesis of zinc oxide nanoparticles: a comparison. *Green Chem Lett Rev*. 2019;12(1):19–24. doi:10.1080/17518253.2018.1547925
48. Nethravathi PC, Shruthi GS, Suresh D, Udayabhanu, Nagabhushana H, Sharma SC, Sharma SC. Garcinia xanthochymus mediated green synthesis of ZnO nanoparticles: photoluminescence, photocatalytic and antioxidant activity studies. *Ceram Int*. 2015;41(7):8680–8687. doi:10.1016/j.ceramint.2015.03.084
49. Saranya KS, Vellora Thekkae Padil V, Senan C, et al. Green synthesis of high temperature stable anatase titanium dioxide nanoparticles using gum kondagogu: characterization and solar driven photocatalytic degradation of organic dye. *Nanomaterials*. 2018;8(12):1002. doi:10.3390/nano8121002
50. Wagh SS, Kadam VS, V. JC, et al. Comparative studies on synthesis, characterization and photocatalytic activity of Ag doped ZnO nanoparticles. *ACS Omega*. 2023;8(8):7779–7790. doi:10.1021/acsomega.2c07499
51. Elbrolesy A, Abdou Y, Elhussiny FA, Morsy R. Novel green synthesis of UV-sunscreen ZnO nanoparticles using Solanum *lycopersicum* fruit extract and evaluation of their antibacterial and anticancer activity. *J Inorg Organomet Polym Mater*. 2023;33(12):3750–3759. doi:10.1007/s10904-023-02744-3
52. Raza A, Sayeed K, Naaz A, et al. Green synthesis of ZnO nanoparticles and Ag-doped ZnO nanocomposite utilizing Sansevieria trifasciata for high-performance asymmetric supercapacitors. *ACS Omega*. 2024;9(30):32444–54. doi:10.1021/acsomega.3c10060
53. Faisal S, Jan H, Shah SA, et al. Green synthesis of zinc oxide (ZnO) nanoparticles using aqueous fruit extracts of myristica fragrans: their characterizations and biological and environmental applications. *ACS Omega*. 2021;6(14):9709–9722. doi:10.1021/acsomega.1c00310
54. MuthuKathija M, Badhusha MSM, Rama V. Green synthesis of zinc oxide nanoparticles using Pisonia Alba leaf extract and its antibacterial activity. *Appl Surf Sci Adv*. 2023;15:100400. doi:10.1016/j.apsadv.2023.100400
55. Tawale JS, Dey KK, Pasricha R, Sood KN, Srivastava AK. Synthesis and characterization of ZnO tetrapods for optical and antibacterial applications. *Thin Solid Films*. 2010;519(3):1244–1247. doi:10.1016/j.tsf.2010.08.077
56. El-Naggar ME, Shaarawy S, Hebeish AA. Bactericidal finishing of loomstate, scoured and bleached cotton fibres via sustainable in-situ synthesis of silver nanoparticles. *Int J Biol Macromol*. 2018;106:1192–1202. doi:10.1016/j.ijbiomac.2017.08.127
57. Raghupathi KR, Koodali RT, Manna AC. Size-dependent bacterial growth inhibition and mechanism of antibacterial activity of zinc oxide nanoparticles. *Langmuir*. 2011;27(7):4020–4028. doi:10.1021/la104825u
58. Ahmad W, Kalra D. Green synthesis, characterization and anti microbial activities of ZnO nanoparticles using Euphorbia hirta leaf extract. *J King Saud Univ - Sci*. 2020;32(4):2358–2364. doi:10.1016/j.jksus.2020.03.014
59. Roy A, Bulut O, Some S, Mandal AK, Yilmaz MD. Green synthesis of silver nanoparticles: biomolecule-nanoparticle organizations targeting antimicrobial activity. *RSC Adv*. 2019;9(5):2673–2702. doi:10.1039/c8ra08982e
60. Sirelkhatim A, Mahmud S, Seeni A, et al. Review on zinc oxide nanoparticles: antibacterial activity and toxicity mechanism. *Nano-Micro Lett*. 2015;7(3):219–242. doi:10.1007/s40820-015-0040-x
61. Saleemi MA, Alallam B, Yong YK, Lim V. Synthesis of zinc oxide nanoparticles with bioflavonoid rutin: characterisation, antioxidant and antimicrobial activities and in vivo cytotoxic effects on artemia nauplii. *Antioxidants*. 2022;11(10). doi:10.3390/antiox11101853
62. Alam S, Rashid MA, Sarker MMR, et al. Antidiarrheal, antimicrobial and antioxidant potentials of methanol extract of Colocasia gigantea Hook. f. leaves: evidenced from in vivo and in vitro studies along with computer-aided approaches. *BMC Complement Med Ther*. 2021;21(1):1–12. doi:10.1186/s12906-021-03290-6
63. Suresh D, Nethravathi PC, Udayabhanu, Rajanaika H, Nagabhushana H, Sharma SC. Green synthesis of multifunctional zinc oxide (ZnO) nanoparticles using Cassia fistula plant extract and their photodegradative, antioxidant and antibacterial activities. *Mater Sci Semicond Process*. 2015;31:446–454. doi:10.1016/j.mssp.2014.12.023
64. Muthuvel A, Jothibas M, Manoharan C. Effect of chemically synthesis compared to biosynthesized ZnO-NPs using Solanum nigrum leaf extract and their photocatalytic, antibacterial and in-vitro antioxidant activity. *J Environ Chem Eng*. 2020;8(2):103705. doi:10.1016/j.jece.2020.103705
65. Murali M, Mahendra C, Nagabhushan, et al. Antibacterial and antioxidant properties of biosynthesized zinc oxide nanoparticles from Ceropegia candelabrum L. – an endemic species. *Spectrochim Acta - Part a mol Biomol Spectrosc*. 2017;179:104–109. doi:10.1016/j.saa.2017.02.027
66. Vijayakumar S, Vaseeharan B, Malaikozhundan B, Shobiya M. Laurus nobilis leaf extract mediated green synthesis of ZnO nanoparticles: characterization and biomedical applications. *Biomed Pharmacother*. 2016;84:1213–1222. doi:10.1016/j.biopha.2016.10.038
67. Saravanan R, Gupta VK, Narayanan V, Stephen A. Comparative study on photocatalytic activity of ZnO prepared by different methods. *J mol Liq*. 2013;181:133–141. doi:10.1016/j.molliq.2013.02.023
68. Mousa SA, Wissa DA, Hassan HH, Ebnalwaled AA, Khairy SA. Enhanced photocatalytic activity of green synthesized zinc oxide nanoparticles using low-cost plant extracts. *Sci Rep*. 2024;14(1):16713. doi:10.1038/s41598-024-66975-1
69. Rezapour M, Talebian N. Comparison of structural, optical properties and photocatalytic activity of ZnO with different morphologies: effect of synthesis methods and reaction media. *Mater Chem Phys*. 2011;129(1–2):249–255. doi:10.1016/j.matchemphys.2011.04.012
70. Mukherji S, Bharti S, Shukla G, Mukherji S. Synthesis and characterization of size-and shape-controlled silver nanoparticles. *Phys Sci Rev*. 2019;4(1):20170082.
71. lvarez-Chimal R, Garca-Prez VI, lvarez-Prez MA, et al. Influence of the particle size on the antibacterial activity of green synthesized zinc oxide nanoparticles using Dysphania ambrosioides extract, supported by molecular docking analysis. *Arab J Chem*. 2022;15(6):103804. doi:10.1016/j.arabjc.2022.103804
72. Pradeev Raj K, Sadaiyandi K, Kennedy A, et al. Influence of Mg doping on ZnO nanoparticles for enhanced photocatalytic evaluation and antibacterial analysis. *Nanoscale Res Lett*. 2018;13:1–13. doi:10.1186/s11671-018-2643-x
73. Alam S, Richi FT, Hasnat H, et al. Chemico-pharmacological evaluations of the dwarf elephant ear (Colocasia affinis Schott) plant metabolites and extracts: health benefits from vegetable source. *Front Pharmacol*. 2024;15: 1428341. doi:10.3389/fphar.2024.1428341
74. Robaczewska J, Kedziora-Kornatowska K, Kozakiewicz M, et al. Role of glutathione metabolism and glutathione-related antioxidant defense systems in hypertension. *J Physiol Pharmacol*. 2016;67(3):331–337.

75. Ahmad H, Sharma R, Mansour A, Awasthi YC. t-Butylated hydroxytoluene enhances intracellular levels of glutathione and related enzymes of rat lens in vitro organ culture. *Exp Eye Res*. 1992;54(1):41–48. doi:10.1016/0014-4835(92)90067-3
76. Canh Pham E, Truong TN. Design, microwave-assisted synthesis, antimicrobial and anticancer evaluation, and in silico studies of some 2-naphthamide derivatives as DHFR and VEGFR-2 Inhibitors. *ACS Omega*. 2022;7(37):33614–33628. doi:10.1021/acsomega.2c05206
77. Kalogris C, Garulli C, Pietrella L, et al. Sanguinarine suppresses basal-like breast cancer growth through dihydrofolate reductase inhibition. *Biochem Pharmacol*. 2014;90(3):226–234. doi:10.1016/j.bcp.2014.05.014
78. Jayaraman P, Sakharkar KR, Lim C, Siddiqi MI, Dhillon SK, Sakharkar MK. Novel phytochemical antibiotic conjugates as multitarget inhibitors of *Pseudomononas aeruginosa* GyrB/ParE and DHFR. *Drug Des Devel Ther*. 2013;7:449–475. doi:10.2147/DDDT.S43964
79. Chauhan A, Verma R, Kumari S, et al. Photocatalytic dye degradation and antimicrobial activities of Pure and Ag-doped ZnO using Cannabis sativa leaf extract. *Sci Rep*. 2020;10(1):1–16. doi:10.1038/s41598-020-64419-0
80. Keerthana S, Kumar A. Potential risks and benefits of zinc oxide nanoparticles: a systematic review. *Crit Rev Toxicol*. 2020;50(1):47–71. doi:10.1080/10408444.2020.1726282
81. Huang H, Feng W, Chen Y, Shi J. Inorganic nanoparticles in clinical trials and translations. *Nano Today*. 2020;35:100972. doi:10.1016/j.nantod.2020.100972